

INVESTIGATING THE PYRO-OPTIC PROPERTIES  
OF  
ANTIMONY SULFO-IODIDE (SbSI)

THESIS

Presented to the Graduate Council  
of Texas State University-San Marcos  
in Partial Fulfillment  
of the Requirements

for the Degree

Master of SCIENCE

by

Eric Osei – Yiadom, B.S.

San Marcos, Texas  
December 2006

**COPYRIGHT**

by

Eric Osei – Yiadom, B.S.

2006

## ACKNOWLEDGEMENTS

I would first like to thank God for taking me through all these years. I would also like to thank my family and friends for all the support that was given me to me throughout all these years. Special thanks go to fiancée Afua Danso for all her support, pieces of advice and love through all these years. I would also like to thank the entire faculty at the Texas State University-San Marcos Department of Physics, especially Dr. David Donnelly, Dr. Wilhelmus Geerts, and Dr. Victor Michalk for being members of my thesis committee and spending some time proofreading my work. Another thanks go to Dr David Donnelly for guiding me through this research work. Special thanks go to the late Dr James Crawford, Nelson Koeck, and Pat Parks for all of the assistance and guidance throughout this journey. Without them, days would have seemed longer. I would also like to thank Kwame Owusu-Adom, James McDonald and William Gibson for all of the assistance throughout college and into the future.

This manuscript was submitted on November 3, 2006.

## TABLE OF CONTENTS

	<b>Page</b>
ACKNOWLEDGEMENT.....	iv
LIST OF TABLES.....	vi
LIST OF FIGURES.....	vii
ABSTRACT.....	ix
CHAPTER .....	1
1. INTRODUCTION.....	1
2. THEORY AND PREVIOUS WORK.....	3
Ferroelectrics.....	3
Theory (Fourier Transform Infrared Spectroscopy).....	8
Previous Work.....	13
3. EXPERIMENTAL PROCEDURE.....	15
The Equipment.....	15
Mounting Sample and Collecting Data.....	19
4. DATA.....	23
5. RESULTS AND CONCLUSION.....	33
Suggestions .....	35
APPENDIX.....	36
REFERENCES.....	44

## LIST OF TABLES

	<b>Page</b>
Table 1. Beamsplitter–detector combinations.....	18

## LIST OF FIGURES

Figure	Page
1. Barium titanate cubic crystal structure above 130 °C.....	4
2. BaTiO <sub>3</sub> has different crystal structures above and below 130 °C.....	5
3. Piezoelectric properties of BaTiO <sub>3</sub> below its Curie temperature.....	7
4. Pyroelectric effect.....	7
5. Michelson Interferometer.....	8
6. Inside the Nicolet 6700 FT-IR Spectrometer.....	16
7. Michelson interferometer showing different mirror positions.....	17
8. Temperature controller and cryogenic equipment.....	19
9. Coldfinger with sample in sample compartment.....	22
10. Transmittance spectrum for SbSI at 9 °C.....	24
11. Transmittance spectrum for SbSI at 10 °C.....	24
12. Transmittance spectrum for SbSI at 11 °C.....	25
13. Transmittance spectrum for SbSI at 12 °C.....	25
14. Transmittance spectrum for SbSI at 13 °C.....	26
15. Transmittance spectrum for SbSI at 14 °C.....	26
16. Transmittance spectrum for SbSI at 15 °C.....	27
17. Transmittance spectrum for SbSI at 16 °C.....	27
18. Transmittance spectrum for SbSI at 17 °C.....	28
19. Transmittance spectrum for SbSI at 18 °C.....	28

20. Transmittance spectrum for SbSI at 19 °C.....	29
21. Transmittance spectrum for SbSI at 20 °C.....	29
22. Transmittance spectrum for SbSI at 21 °C.....	30
23. Transmittance spectrum for SbSI at 22 °C.....	30
24. Transmittance spectrum for SbSI at 23 °C.....	31
25. Transmittance spectrum for SbSI at 24 °C.....	31
26. Transmittance spectrum for SbSI from 9 °C to 24 °C.....	32

## ABSTRACT

### INVESTIGATING THE PYRO-OPTIC PROPERTIES OF ANTIMONY SULFO – IODIDE (SbSI)

by

Eric Osei – Yiadom, B.S.

Texas State University–San Marcos

December 2006

SUPERVISING PROFESSOR: DAVID DONNELLY

In this study, we investigated the pyro-optic properties of Antimony Sulfo-Iodide (SbSI) film. Using the Nicolet 6700 FT-IR Spectrometer, absorbance spectra were obtained for the SbSI film. Repeated spectra were obtained over time as the SbSI film was subjected to temperature ranging of 9 °C – 24 °C at 1 °C increment. From these absorbance spectra, transmittance spectra were then obtained. The transmittance is determined to be dependent on temperature which predicts that SbSI films can be used as an infrared detector. The pyro-optic coefficient is estimated to be around  $7.08 \times 10^{-4} \text{ } ^\circ\text{C}^{-1}$  below the Curie temperature and  $0.12 \text{ } ^\circ\text{C}^{-1}$  above the Curie temperature. The ferroelectric property of a crystallographic phase change is also observed, as SbSI is a ferroelectric material.

## CHAPTER 1

### INTRODUCTION

Infrared imaging devices capable of operating in the range of 2-14 microns are of interest for a large number of applications in commercial as well as in military sectors. Currently commercially available imaging devices are either photon detectors or pyroelectric detectors. Both have their advantages as well as disadvantages. Photon detectors are very accurate but must be cooled to liquid nitrogen temperature (77 K) for efficient operation. Thus these devices are bulky and costly. On the other hand pyroelectric detectors operate at room temperature which eliminates the use of cryogenic coolants in the system. However, they too have shortcomings such as electronic noise due to metallic contacts to pixel elements in the array; and need of thermal isolation between the pyroelectric elements and the read-out integrated circuits (ROIC).

Detectors utilizing pyro-optic effect offer an alternative to uncooled pyroelectric detectors. Many ferroelectric materials exhibit the pyro-optic effect with peak response around the transition temperature. The pyro-optic effect is optical in nature and is defined as

$$J = \frac{dn}{dT} \quad (1.1)$$

That is, the induced refractive index (n) caused by thermal gradient (dT) to which a pyro-optic sample is subjected. The refractive index is anisotropic and is a temperature

dependent parameter of materials. The purpose of this research was to investigate the pyro-optic properties of Antimony Sulfo – Iodide (SbSI) and to determine if it's an appropriate material for use as an infrared detector, because it is one of the ferroelectric materials which exhibit the pyro-optic effect. Antimony Sulfo-Iodide belongs to the compounds with general formula  $A^V B^{VI} C^{VII}$  (where A=Sb; B=S, Se; and C=Cl, Br, I) and V, VI, VII are groups five, six and seven respectively on the periodic table). Antimony Sulfo-Iodide (SbSI) is of interest because of its ferroelectric and semi-conducting properties and its potential as an infrared detector. High values of spontaneous polarization  $P_S$ ,  $T_C$  (Curie temperature) near room temperature and rather small energy gap  $E_g$  in comparison with other ferroelectrics are the important features of SbSI [1]. In the crystal form, SbSI has a Curie temperature of  $\sim 22^\circ\text{C}$ , while in the form of a film it has a Curie temperature of  $\sim 19^\circ\text{C}$  [2]. Curie temperature is defined as the temperature at which a ferroelectric material undergoes a crystallographic phase change from an asymmetrical, non-centrosymmetric structure to a centrosymmetric crystal structure, thus losing its spontaneous polarization [3]. A thorough understanding of the pyro-optic effect and other properties is essential in using SbSI as an infrared detector.

The following chapters describe a study of the pyro-optic effect on SbSI. Chapter 2 introduces some of the properties of SbSI and the laboratory instrumentation used in this study. It also delves into some previous work that has been done on SbSI. Chapter 3 describes the experimental procedure used. In chapter 4, the data are presented. Chapter 5 gives results, conclusions and suggestions for additional studies.

## CHAPTER 2

### THEORY AND PREVIOUS WORK

#### Ferroelectrics

SbSI is of interest in this research also because of its ferroelectric properties. In a normal dielectric, upon the application of an electric field, positive and negative charges will be displaced from their original position – a concept which is characterized by the dipole moment or polarization. The polarization or displacement will vanish, however, when the electric field returns back to zero. In a ferroelectric material, on the other hand, there is a spontaneous polarization – a displacement which is inherent to the crystal structure of the material and does not disappear in the absence of the electric field. In addition, the direction of this polarization can be reversed or reoriented by applying an appropriate electric field [4]. All ferroelectric crystals are necessarily both pyroelectric and piezoelectric. Many lose these polar properties at the transition or Curie temperature  $T_c$ . A nonpolar phase above  $T_c$  is the so-called paraelectric phase. Barium titanate ( $\text{BaTiO}_3$ ) is probably the best cited example. Above approximately 130 °C, the crystal structure of  $\text{BaTiO}_3$  has a cubic unit cell as shown in the figure below.

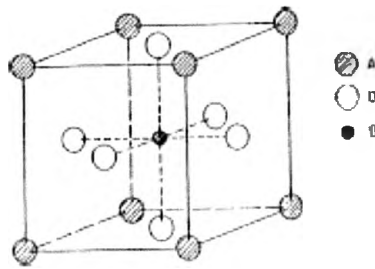


**Figure 1. Barium titanate cubic crystal structure above 130 °C [4].**

A – Ba<sup>2+</sup>, O – O<sup>2-</sup>, B – Ti<sup>4+</sup>

The centers of mass of the negative charges (O<sup>2-</sup>) and the positive charges, Ba<sup>2+</sup> and Ti<sup>4+</sup>, coincide at the Ti<sup>4+</sup> ion. There is therefore no net polarization and  $\mathbf{P}=0$ . Above 130 °C, therefore, the barium titanate crystal exhibits no permanent polarization and is not ferroelectric. However, below 130 °C, the structure of barium titanate is tetragonal, in which the Ti<sup>4+</sup> atom is not located at the center of mass of the negative charges. The crystal is therefore polarized by the separation of the centers of mass of the negative and positive charges. The crystal possesses a finite polarization vector  $\mathbf{P}$  and is ferroelectric.

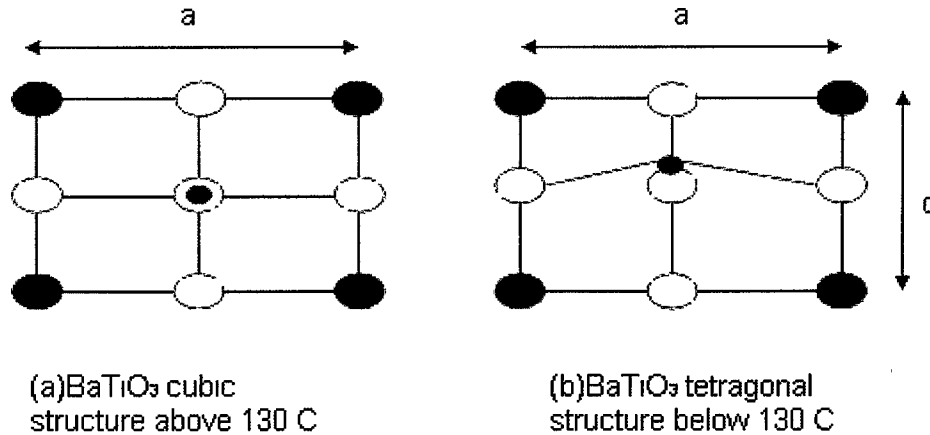


**Figure 2. BaTiO<sub>3</sub> has different crystal structures above and below 130 °C.**

Below the Curie temperature, the whole crystal becomes spontaneously polarized. The onset of spontaneous polarization is accompanied by the distortion of the crystal structure, as shown in the Fig. 2(a) to Fig. 2(b). The spontaneous displacement of the Ti<sup>4+</sup> ion below the Curie temperature elongates the cubic structure, which becomes tetragonal. The development of the permanent dipole moment below the Curie temperature involves long-range interactions between the ions outside the simple unit cell. The energy of the crystal is lower when the Ti<sup>4+</sup> ion in each unit cell is slightly displaced along the c direction as in Fig. 2(b) above, which generates a dipole moment in each unit cell. The interaction energy of these dipoles when all are aligned in the same direction lowers the energy of the whole crystal. It should be mentioned that the distortion of the crystal that takes place when spontaneous polarization occurs just below  $T_c$  is very small relative to the dimensions of the unit cell. For BaTiO<sub>3</sub>, for example,  $c/a$  is 1.01 and the displacement of Ti<sup>4+</sup> ion from the center is only 0.012 nm, compared with  $a = 0.4$  nm.

An important and technologically useful characteristic of a ferroelectric crystal is its ability to be poled. Above 130 °C there is no permanent polarization in the crystal. If we apply a temporary field  $E$  and let the crystal cool to below 130 °C, we can induce the spontaneous polarization  $\mathbf{P}$  to develop along the field direction. In other words, we would define the  $c$  axis by imposing a temporary external field. This process is called poling. The  $c$  axis is the polar axis along which  $\mathbf{P}$  develops. It is also called the **ferroelectric axis**. Since below the Curie temperature the ferroelectric crystal already has a permanent polarization, it is not possible to use the expression

$$P = \epsilon_o(\epsilon_r - 1)E \quad (2.1)$$

to define a relative permittivity. Suppose that we use a ferroelectric crystal as a dielectric medium between two parallel plates. Since any change  $\Delta P$  normal to the plates changes the stored charge, what is of significance to the observer is the change in the polarization. We can appreciate this by noting that  $C = Q/V$  is not a good definition of capacitance if there are already charges on the plates, even in the absence of voltage. We then prefer a definition of  $C$  based on  $\Delta Q/\Delta V$  where  $\Delta Q$  is the change in stored charge due to a change  $\Delta V$  in the voltage. Similarly, we define the relative permittivity  $\epsilon_r$ , in this case in terms of the change  $\Delta P$  in  $\mathbf{P}$  induced by  $\Delta E$  in the field  $E$ ,

$$\Delta P = \epsilon_o(\epsilon_r - 1)\Delta E \quad (2.2)$$

Ferroelectrics are also said to be pyroelectric because when the temperature increases, the crystal expands and the relative distances of ions change, which result in a change in polarization. Thus, an electrical potential is created when they are heated, that is, a temperature change  $\Delta T$  induces a change  $\Delta P$  in the polarization of the crystal. A

material that exhibits such an effect is  $\text{BaTiO}_3$ . This is illustrated in the figure below. The magnitude of this effect is quantized by the pyroelectric coefficient  $p$ , which is defined by

$$p = \frac{dP}{dT} \quad (2.3)$$

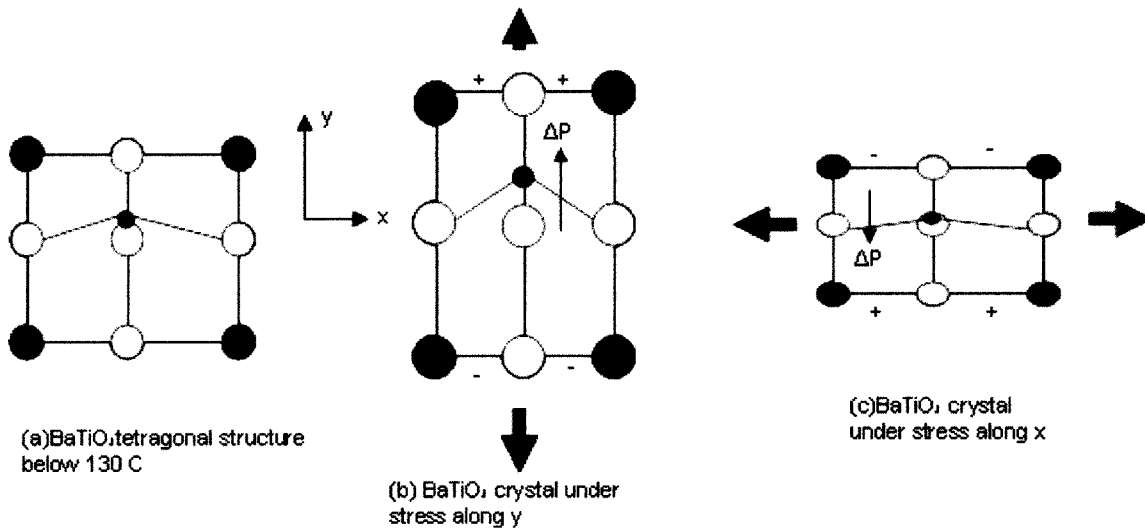


Figure 3. Piezoelectric properties of  $\text{BaTiO}_3$  below its Curie temperature.

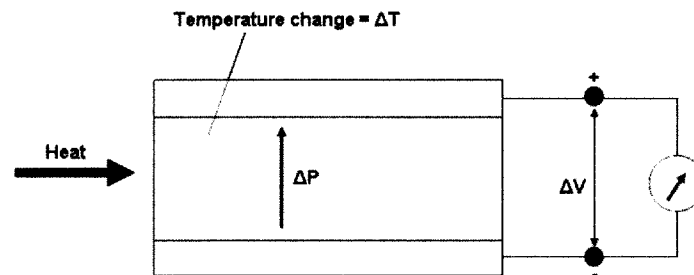


Figure 4. Pyroelectric effect.

Some ferroelectric materials are said to be piezoelectric because on the application of mechanical stress or when strained, the material develops an internal field and therefore exhibits a voltage difference between two of its faces.

## Theory (Fourier Transform Infrared Spectroscopy)

The instrument used to collect and process data for this study was the FTIR part of the NXR FT-Raman Spectrometer which was manufactured by Thermo Electron Corporation. Fourier Transform Infrared Spectroscopy (FTIR) uses a wide spectrum infrared (IR) source to identify vibrational modes associated with chemical bonds in a substance. The basic optical component of Fourier transform spectrometers is the Michelson interferometer. Light from an infrared source – a heated element or a glowbar – is collimated and directed on a beam splitter. An ideal beam splitter creates two separate optical paths by reflecting 50% of the incident light and transmitting the remaining 50%. Although light from the source is incoherent, when it is split into two components by the beam splitter, the components are coherent and can produce interference phenomena when the beams are recombined. In the near and middle infrared region, germanium deposited on KBr substrate is commonly used as beam splitter.

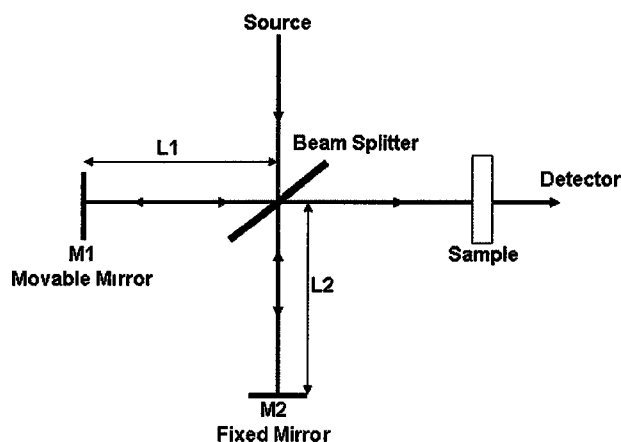


Figure 5. Michelson Interferometer.

The intensity reaching the detector is the sum of the two beams. The two beams are in phase and reinforce each other when  $L_1=L_2$ . When M1 is moved, the optical

path lengths are unequal and an optical path difference  $\delta$  is introduced. If M1 is moved a distance  $x$ , the retardation is  $\delta=2x$  since the light has to travel an additional distance  $x$  to reach the mirror and the same additional distance to reach the beam splitter.

Consider the output signal from the detector when the source emits a single frequency or wavelength. For  $L_1=L_2$  the two beams reinforce each other because they are in phase,  $\delta=0$ , and the detector output is a maximum. If M1 is moved by  $x = \lambda/4$ , the retardation becomes  $\delta = 2x = \lambda/2$ . The two wavefronts reach the detector  $180^\circ$  out of phase, resulting in destructive interference or zero output. For an additional  $\lambda/4$  movement by M1,  $\delta=\lambda$  and constructive interference results again. For an input beam of monochromatic light of frequency  $f$  and intensity  $B(f)$ , the intensity of the interferogram as a function of the optical path difference  $x$  between the two beams is given by the familiar two-beam interference relation for the intensity [5],

$$I_o(x) = B(f_o)[1 + \cos(2\pi x f_o)] \quad (2.4)$$

Where  $B(f_o)$  is the source intensity modified by the sample. When the source emits more than one frequency, the detector sees a superposition of cosines and Eq. (2.4) is replaced by the integration

$$I_o(x) = \int_0^{\infty} B(f)[1 + \cos(2\pi x f)]df \quad (2.5)$$

We can subtract the mean value of the interferogram and form an expression for the intensity as a function of  $x$ :

$$I(x) = I_o(x) - \overline{I(x)} = \int_0^{\infty} B(f) \cos(2\pi x f) dx \quad [6] (2.6)$$

The right-hand side contains all the spectral information in the light and is the cosine Fourier transform of the source distribution  $B(f)$ . The distribution can therefore be recovered by the inverse Fourier transform,

$$B(f) = \int_0^{\infty} I(x) \cos(2\pi fx) dx \quad (2.7)$$

What is measured in FTIR spectroscopy is the interferogram, containing not only the spectral information of source, but also the transmittance characteristics of the sample. An interferogram is generated because of the unique optics of an FT-IR instrument. The key components are a moveable mirror and beam splitter. The moveable mirror is responsible for the quality of the interferogram, and it is very important to move the mirror at constant speed. As the movable mirror travels, different frequencies are reflected in different ways. The summation of constructive and destructive interference over time makes the interferogram, from which a Fourier transform is used to calculate the spectrum. The interferogram is a plot of infrared intensity versus optical path difference, which can be measured in cm. By its very nature, when a function is Fourier transformed its X axis units are inverted. The Fourier transform of an interferogram produces a plot of infrared intensity versus inverse centimeters, or  $\text{cm}^{-1}$ . Inverse centimeters are also known as wavenumbers. A plot of infrared intensity versus wavenumber is an infrared spectrum [7].

The spectrometer operates with wavelengths ranging from 2.5  $\mu\text{m}$  to 25.5  $\mu\text{m}$ . These values are normally reported as wavenumbers of 4000  $\text{cm}^{-1}$  to 400  $\text{cm}^{-1}$ . A wavenumber is defined as the reciprocal of the wavelength as follows:

$$W = 1/\lambda \quad (2.8)$$

Where,  $W$  = wavenumber in  $\text{cm}^{-1}$ ,  $\lambda$  = wavelength in cm.

If  $\lambda$  is measured in cm, then  $W$  is reported as  $\text{cm}^{-1}$ , sometimes called reciprocal centimeters.  $W$  is a measure of the number of cycles in a light wave per centimeter [7].

The FTIR actually measures the absorption of individual wavelengths passing through a substance. This absorption, which is normally reported as percent transmittance or absorbance, is representative of the energy transferred from the photons to the chemical bonds with complimentary vibrational modes. Absorbance is defined as follows:

$$A = \log\left(\frac{I_0}{I}\right) \quad (2.9)$$

Where  $A$  = absorbance

$I$  = light intensity with a sample in the infrared beam (sample spectrum)

$I_0$  = light intensity measured with no sample in the infrared beam (background spectrum).

Transmittance is also defined as follows:

$$T = \frac{I}{I_0} \quad (2.10)$$

Where  $T$  = transmittance

$I$  = light intensity with a sample in the infrared beam (sample spectrum)

$I_0$  = light intensity measured with no sample in the infrared beam (background spectrum).

$$A = -\log_{10} T \quad (2.11)$$

The energy captured by the chemical bonds causes them to vibrate in a predictable fashion. This vibration may be described as a change in the inter-atomic distances known as stretching or a change in the angle between two bonds known as bending. For

polyatomic species, total possible motions =  $3N$  (there are 3 co-ordinates per atom), but 3 specify the position of the molecule and 3 specify the rotation of the molecule, so  $3N-6$  are left for the atoms to vibrate and bend in the molecule, where  $N$  is the number of atoms in the molecule. It is not necessary for the number of vibrational modes detected to equal the maximum number of vibrational modes. More than one vibrational mode may share similar energies, the intensity of the vibrational mode may not be sufficient for detection or it may be outside the range of the detector [8]. The significance of each vibration is that every vibration is caused by a specific wavelength. Since the FTIR is designed to compare the intensity of the source with the intensity transmitted through the sample, it is therefore possible to identify which wavelengths are absorbed by the sample. By comparison of the absorbed wavelengths to known standards of chemical structure, it is possible to identify the species present in the sample [9]. It is also possible to identify the structure of the sample by observation of the absorption peaks to identify the bonds present.

At room temperature, the vast majority of molecules are in the  $V=0$  or ground vibrational state, where  $V$  is the discrete vibrational energy level which is called a vibrational quantum number. When a molecule absorbs infrared light and is excited to the first vibrational energy level ( $V=1$ ), it is said to undergo a fundamental transition. When a molecule is in the  $V=1$  level, it is said to contain one quantum of vibrational energy. The vast majority of molecules in the universe have vibrations for which the  $V=1$  level is  $4000$  to  $400\text{ cm}^{-1}$  in energy higher than the  $V=0$  level. This means that the vast majority of molecules in the universe have infrared bands between  $4000$  and  $400\text{ cm}^{-1}$ . Most of the intense features in any mid-infrared spectrum can be assigned to fundamental transitions.

The wavenumber positions of mid-infrared fundamental bands correlate well with molecular structure, which is why the mid-infrared part of the electromagnetic spectrum is useful [10].

### **Previous Work**

Ferroelectricity of antimony Sulfo-iodide SbSI was discovered in 1962 [11]. Since that time SbSI has been extensively investigated. This interest has been generated by its photoconducting, semiconducting and optical properties on one hand and for its ferroelectric, dielectric and electromechanical properties on the other hand.

Variation of the forbidden gap of SbSI crystals in the phase transition region has been analyzed using the pseudo-potential method for the antiferroelectric and ferroelectric phase. The band gap at several special points of the Brillouin zone and some characteristic parameters of the band were also considered. At the ferroelectric phase transition, the valence and conduction bands change due to displacement of Sb and S atoms with respect to I and with respect to each other as a result of order-disorder and displacement-type transition [12]. In the order-disorder transition, the particles perform oscillations relative to their equilibrium positions, and can also move from one equilibrium position to the other, under the action of random thermal forces, while in the displacement-type transitions the relative distance of ions change due to temperature increase.

Studies on pyro-optic materials for infrared imaging have been done by Jie-Fang Li et al. [13]. In this study, the temperature dependence of the complex refractive indices of SbSI, molybdenum disulfide ( $\text{MoS}_2$ ), and bismuth vanadate ( $\text{BiVO}_4$ ) were investigated using spectroscopic ellipsometry. The wavelength of maximum temperature dependence

was identified for an in depth study of the sensitivity of the reflectance coefficient to a small ac temperature modulation. It was found feasible to detect temperature changes of  $10^{-3}$ ,  $10^{-2}$ , and  $10^{-1}$  °C by monitoring the reflectance coefficient of SbSI, MoS<sub>2</sub>, and BiVO<sub>4</sub>, respectively, using null ellipsometry. It is thus possible to use the pyro-optic phenomena for long wavelength infrared imaging, analogous to pyroelectrics [13].

Due to the various properties of SbSI, some researchers are even investigating SbSI films for fabricating the pyro-optic detector [14].

## **CHAPTER 3**

### **EXPERIMENTAL PROCEDURE**

#### **The Equipment**

The equipment used for this research is the NICOLET 6700 FT-IR manufactured by Thermo Electron Corporation, which is depicted in Fig. 1 below. This uses OMNIC version 6.0. OMNIC is an advanced software package for FTIR spectroscopy that lets you perform a wide range of tasks, from collecting infrared spectra to performing quantitative analysis. The commands needed to collect and process spectra are conveniently arranged in menus and can also be entered from the keyboard using shortcut keys. This spectrometer measures the electromagnetic radiation at particular wavelengths that is absorbed or transmitted by the sample. The infrared radiation is directed to the sample. When the radiation strikes the sample, the sample either absorbs, scatters or transmits this radiation. The spectra produced by the FTIR show the effective absorption or the transmission as a function of the wavelength. If the effect of absorption and scattering on the intensity of the transmitted beam is the same, it will reduce the transmitted beam intensity.

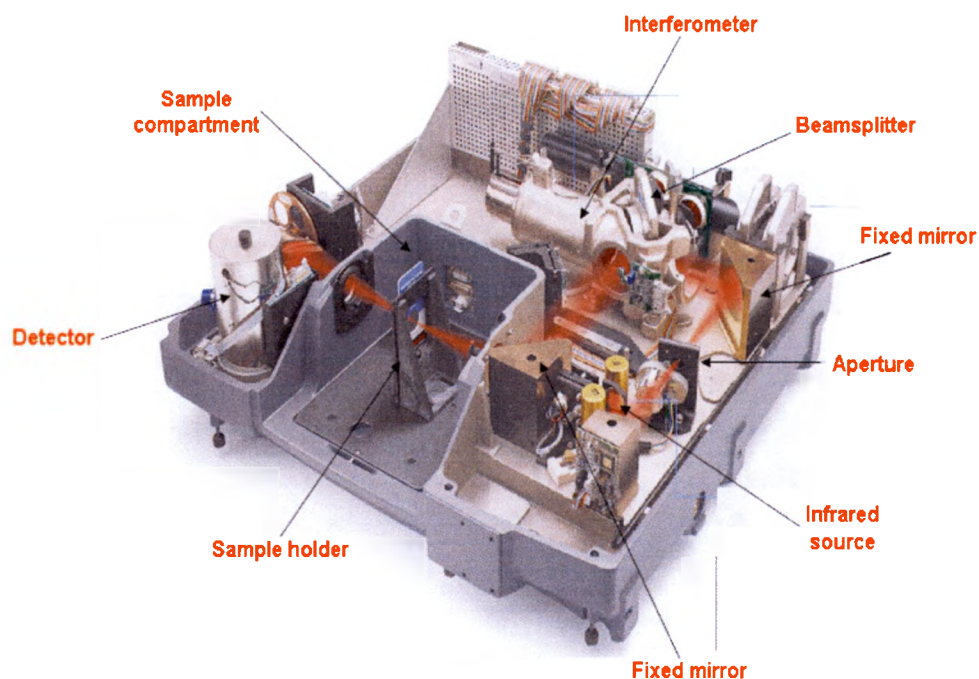


**Figure 6. Inside the Nicolet 6700 FT-IR Spectrometer.**

Infrared radiation from a radiation source is directed toward the Michelson interferometer. This collimated light is then incident on a beam splitter. An ideal beam splitter creates two separate optical paths by transmitting 50% of the incident light and reflecting the remaining 50%. The two beams produce interference when they are recombined. This recombined beam is then directed towards the sample and its rate of effective absorbance or transmittance is recorded, which is represented on the y-axis of the spectra produced by the FT-IR.

The interferometer provides a means for the spectrometer to measure all frequencies simultaneously. The interferometer modulates the intensity of individual frequencies emitted by the sample. The beams are reflected from the surfaces of the two mirrors and recombine at the beamsplitter. When the beams recombine, constructive or destructive interference occurs depending on the position of the moving mirror relative to

the fixed mirror. The illustration shows the signal measured at the detector for a monochromatic or single frequency source.

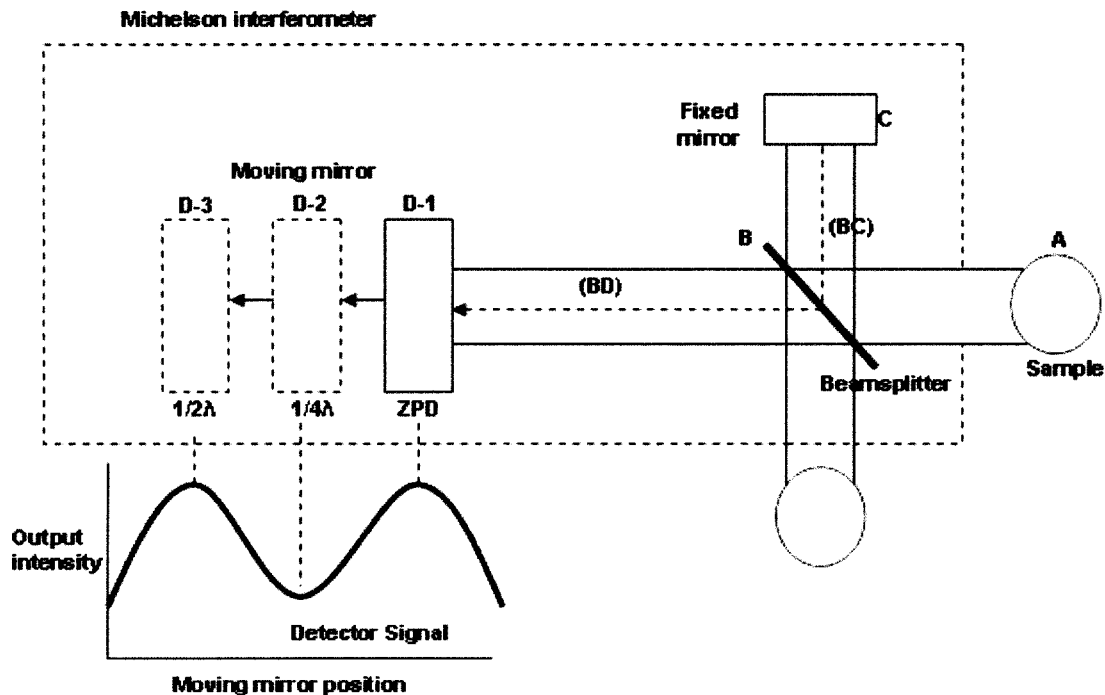


Figure 7. Michelson Interferometer showing different mirror positions.

When both mirrors are the same distance from the beamsplitter, the two beams travel exactly the same path length and, consequently, are totally in phase with each other. The resulting intensity is at its maximum, a point called the zero path difference (ZPD). When the beams recombine to create a strong signal (at mirror positions D-1 and D-3), constructive interference is said to have occurred. When the beams recombine to create a weak signal (at mirror position D-2), destructive interference has occurred. The recombined beam travels to the detector, which translates the beam into an electrical signal that can be processed by the computer. Using a mathematical process called Fourier Transformation (FT), the system computer converts the interferogram into a

spectrum. The spectrum shows the sample emission at all the frequencies measured and thus can be used to identify the sample.

A number of beamsplitters and detectors are available for use in the NXR FT-Raman Spectrometer. There are two considerations when selecting a beamsplitter-detector combination: compatibility and spectral range. Combinations are considered compatible if they provide a detector signal that is large enough to allow the beamsplitter to be aligned. The following table shows which beamsplitter-detector combinations perform best and which are compatible.

DETECTOR	BEAMSPLITTER					
	Near – IR			Mid – IR		Far – IR
	Quartz	CaF <sub>2</sub>	XT-KBr	KBr	CsI	Solid Substrate
DTGS (KBr window)	X	OK	Best	Best	OK	X
DTGS (CsI window)	X	X	OK	OK	Best	X
DTGS (PE window)	X	X	X	X	OK	Best
MCT-A	OK	OK	Best	Best	OK	X
MCT-B	OK	OK	Best	Best	OK	X
InSb	OK	Best	OK	X	X	X
PbSe	OK	Best	Ok	X	X	X
Si	Best	OK	X	X	X	X
PbS	OK	Best	X	X	X	X
InGaAs	OK	Best	OK	X	X	X

**Table 1. Beamsplitter-detector combinations.**

Best = Optimum beamsplitter-detector combination.

OK = Compatible beamsplitter-detector combination.

X = Incompatible beamsplitter-detector combination. [15]

### Mounting Sample and Collecting Data

Spectral readings were to be taken from 9°C to 24°C at 1°C interval and as such the sample needed to be cooled to this low temperature range. Sample temperatures were achieved by mounting the sample on the coldfinger of Cryogenic equipment by Janis Research Co. Inc. and using ice as the coolant. Ice was used because the temperature range was not that extreme to use liquid nitrogen as the coolant. The cryogenic equipment was then connected to a Lakeshore Autotuning Temperature Controller to read the temperature variations so that spectral readings could be done at the required temperatures. The connection of the temperature controller and the cryogenic equipment is shown in Fig. 8 below.

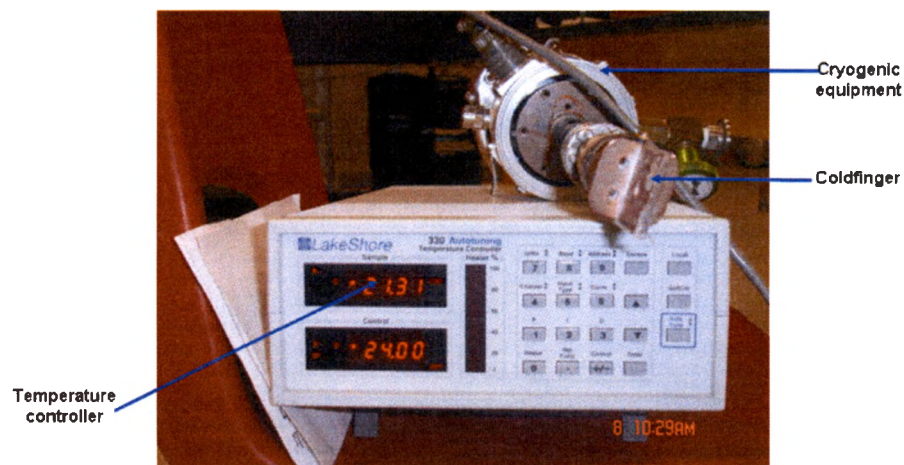
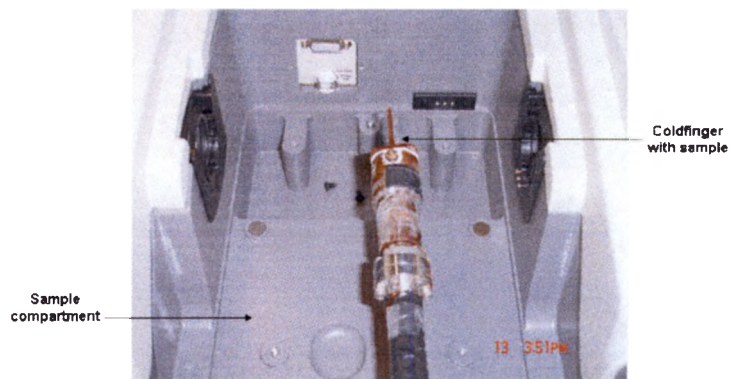


Figure 8. Temperature Controller and Cryogenic equipment.

As the sample's temperature was lowered, the necessary initialization procedures on the spectrometer were performed. In doing so, the spectrometer was purged with liquid N<sub>2</sub> by setting the pressure regulator between 20 and 40 pounds per square inch (psi) and the flow meter to read approximately 30 standard cubic feet per hour (scfh). Purging is done to keep the spectrometer free of undesirable gases, to protect the optics and improve the system's thermal stability. The detector was also cooled by filling the detector fill ports with liquid N<sub>2</sub>. For Fourier transform infrared spectroscopy the basic instrument settings are dictated by the sample. The resolution used for liquid or solid samples is 4 wavenumbers (cm<sup>-1</sup>) to 8 wavenumbers (cm<sup>-1</sup>) while gas samples usually require a resolution of 2 wavenumbers (cm<sup>-1</sup>). The resolution setting is somewhat misleading as it is a complex calculation of the mirror velocity and the spacing of the data points sampled. Therefore, a simpler view may be that a resolution of 4 wavenumbers (cm<sup>-1</sup>) results in data collection at intervals of approximately 1.928 wavenumbers (cm<sup>-1</sup>) and a 5 wavenumbers resolution results in data collection of approximately every 2.48 wavenumbers. In acquiring the data, the spectrometer resolution was set at 4 wavenumbers and the number of scans also chosen to be 64. The number of scans is the number of data points taken at each frequency or step during the scan. These values are then averaged to reduce the noise to signal ratio, but obviously, this reaches a point of diminishing returns at large numbers. The correct combination of the detector and beam splitter was chosen to be MCT-A and XT-KBr respectively. The MCT detector is also called mercury cadmium telluride (HgCdTe) detector. This consists of an alloy of these three elements and it is a semiconductor. The detector element absorbs infrared photons, and as a result electrons are promoted from the valence band (or bonding orbital) to the

conduction band (or anti-bonding orbital). Once electrons are in the conduction band they can respond to an electrical current. The electrical current is a measure of the number of electrons, and so is directly proportional to the number of infrared photons hitting the detector. Thus, the current generated by the detector element is a direct measure of the infrared intensity. Potassium bromide (KBr) is almost universally used as a substrate material in FTIR beamsplitters. Although these beamsplitters are referred to as being made out of KBr, this material does not split the beam since it transmits the infrared. Instead, a thin coating of germanium is sandwiched between two pieces of KBr, and it is this Ge coating that splits the beam [16]. The acquisition of data then began after configuring the spectrometer with these specifications. The first spectrum that was acquired was the background spectrum; this is because a sample spectrum is usually “ratioed” against a background spectrum. The background spectrum measures response of the spectrometer without a sample in place. Dividing the sample spectrum by the background – called “ratioing” – removes the effects caused by the instrument and atmospheric conditions so the peaks in the final spectrum are due solely to the sample.

After cooling the sample to a lower temperature, the cold finger with the sample mounted on it was then placed in the Spectrometer to begin data acquisition. This process is showed in the Fig. 9 below.



**Figure 9. Coldfinger with sample in Sample compartment.**

In acquiring the data, since the sample was cooled to a lower temperature, spectra readings were taken from the smallest temperature and at each increment of 1 °C, data was taken till the temperature reached the required maximum temperature of 24 °C.

## CHAPTER 4

### DATA

The data are presented as absorbance spectra. Absorbance spectra are calculated as

$$A = \log\left(\frac{I_0}{I}\right) \quad (4.1)$$

Where A = absorbance

I = light intensity with a sample in the infrared beam (sample spectrum)

I<sub>0</sub> = light intensity measured with no sample in the infrared beam (background spectrum).

$$A = -\log_{10}(T) \quad (4.2)$$

Where T is the transmittance.

The vertical axis shows % transmittance and the horizontal axis shows wavenumbers (cm<sup>-1</sup>). All spectra have a resolution of 4 cm<sup>-1</sup>.

Figures 10 through 26 are the various spectra taken for varying temperatures from 9 °C to 24 °C.

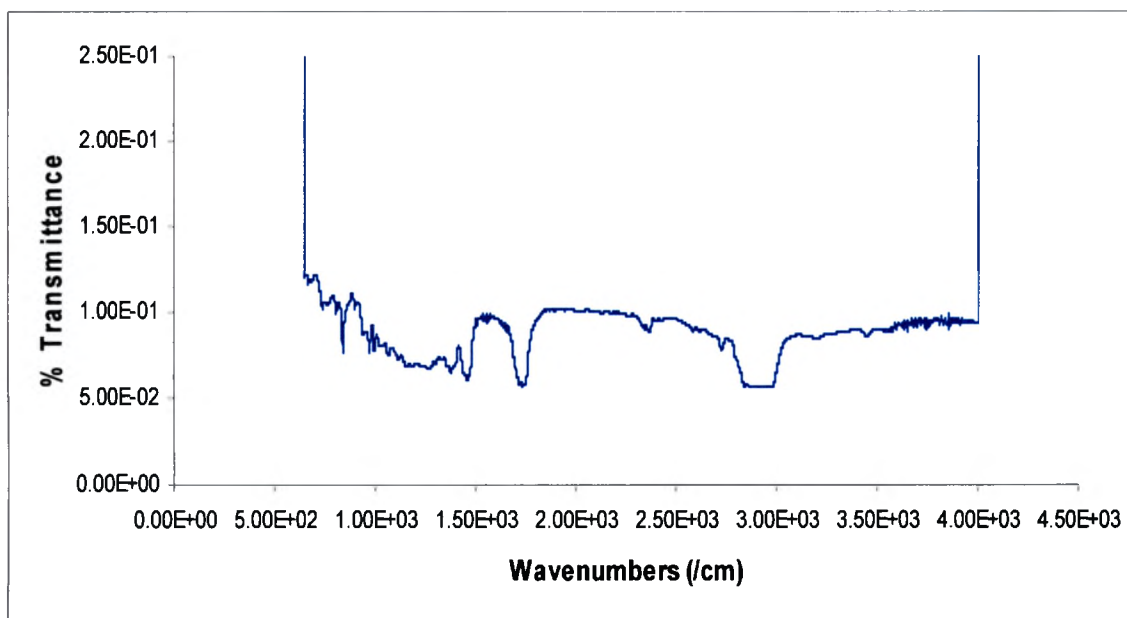


Figure 10. Transmittance Spectrum for SbSI at 9 °C.

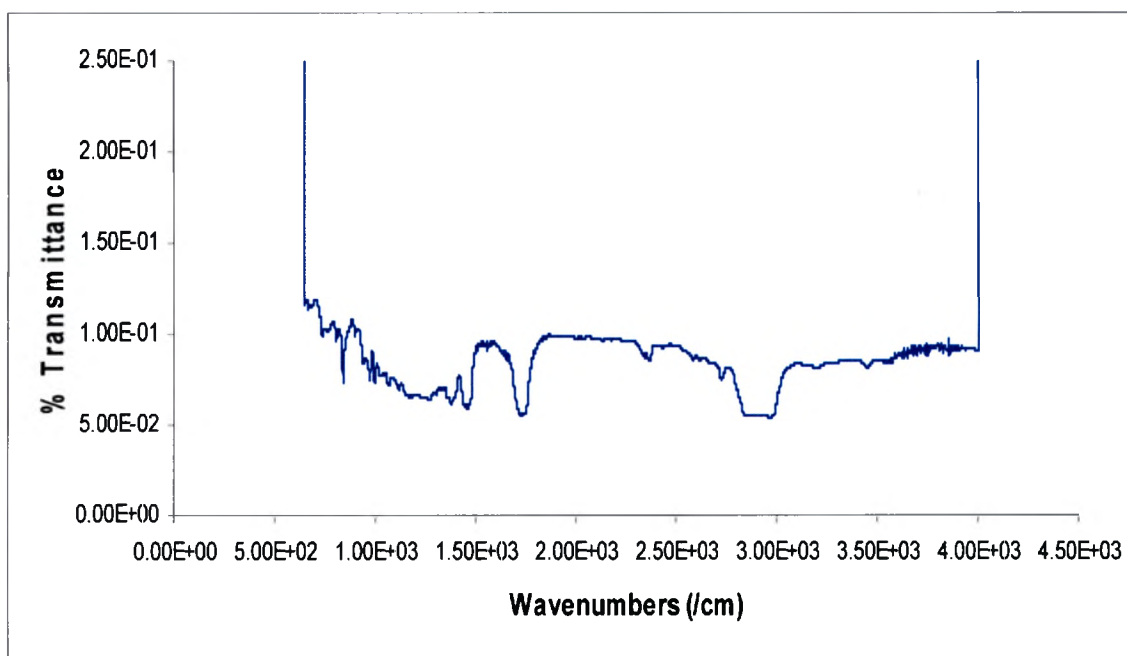


Figure 11. Transmittance Spectrum for SbSI at 10 °C.

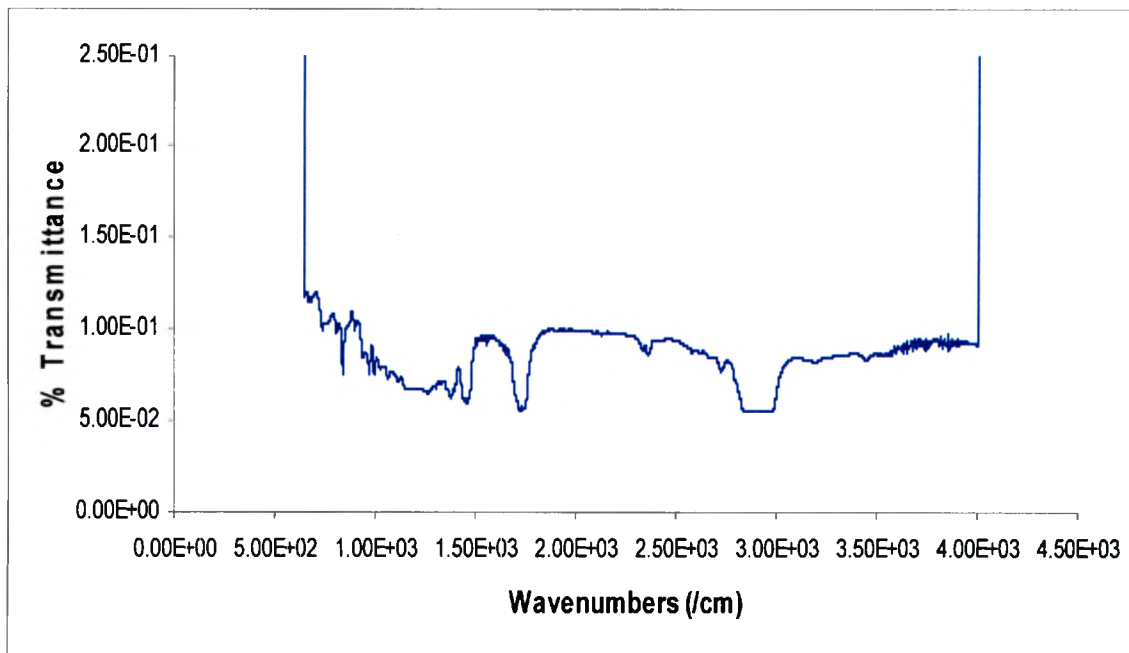


Figure 12. Transmittance Spectrum for SbSI at 11 °C.

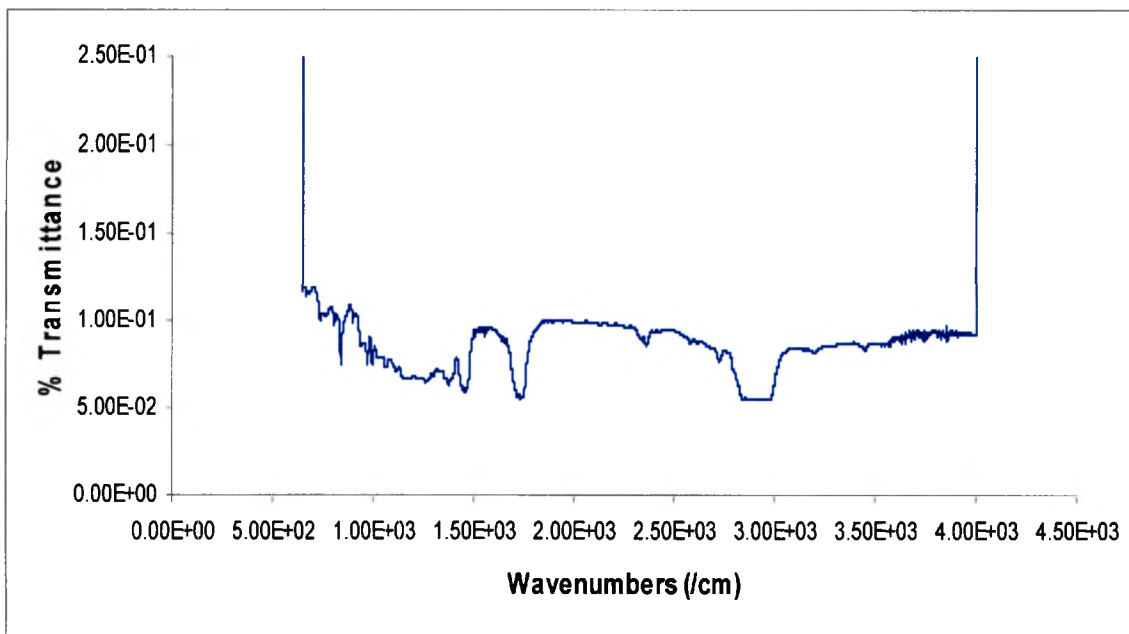


Figure 13. Transmittance Spectrum for SbSI at 12 °C.

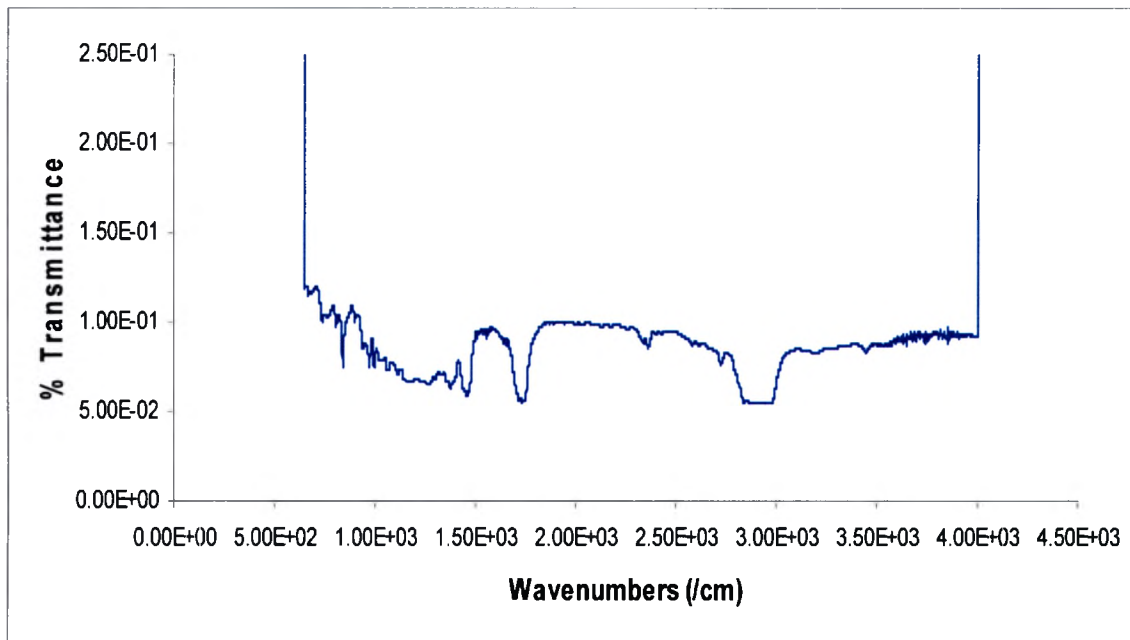


Figure 14. Transmittance Spectrum for SbSI at 13 °C.

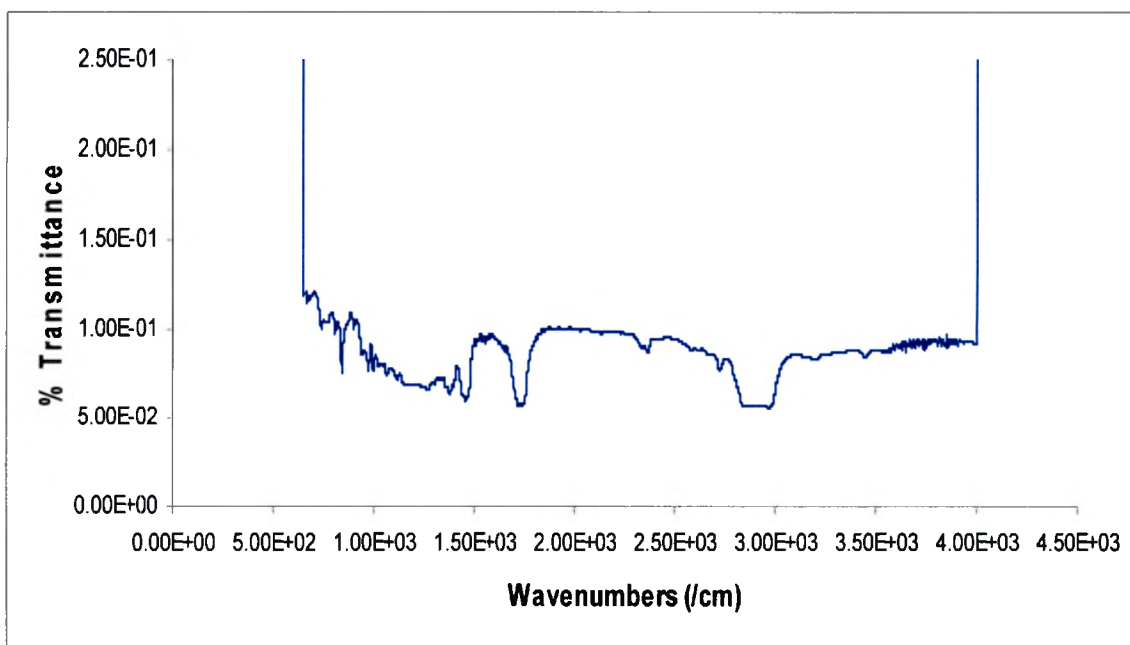


Figure 15. Transmittance Spectrum for SbSI at 14 °C.

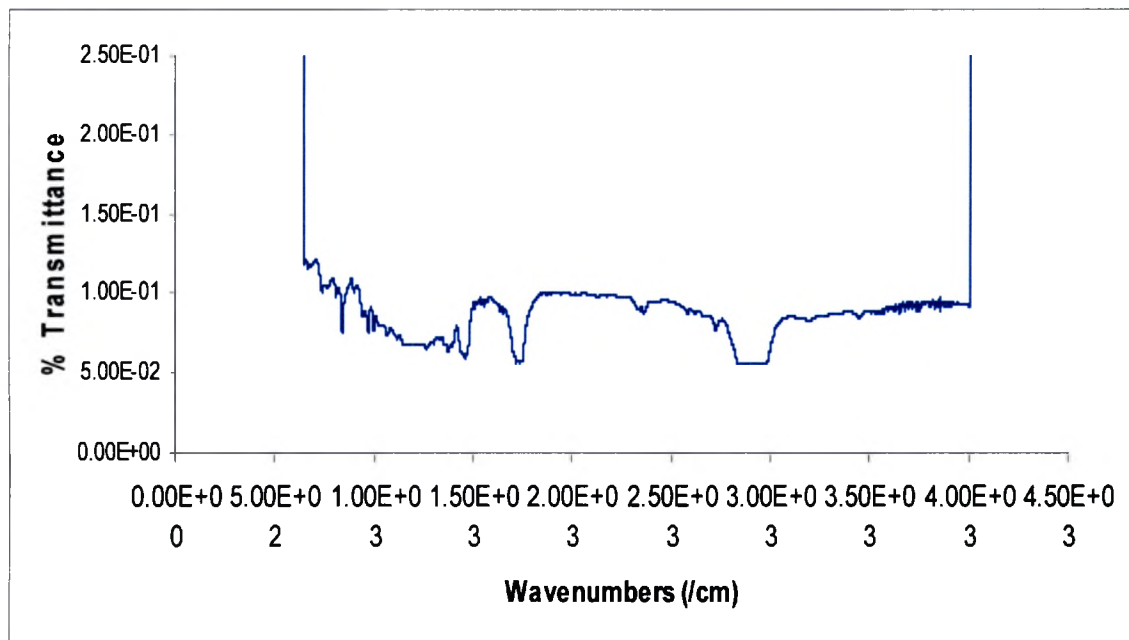


Figure 16. Transmittance Spectrum for SbSI at 15 °C.

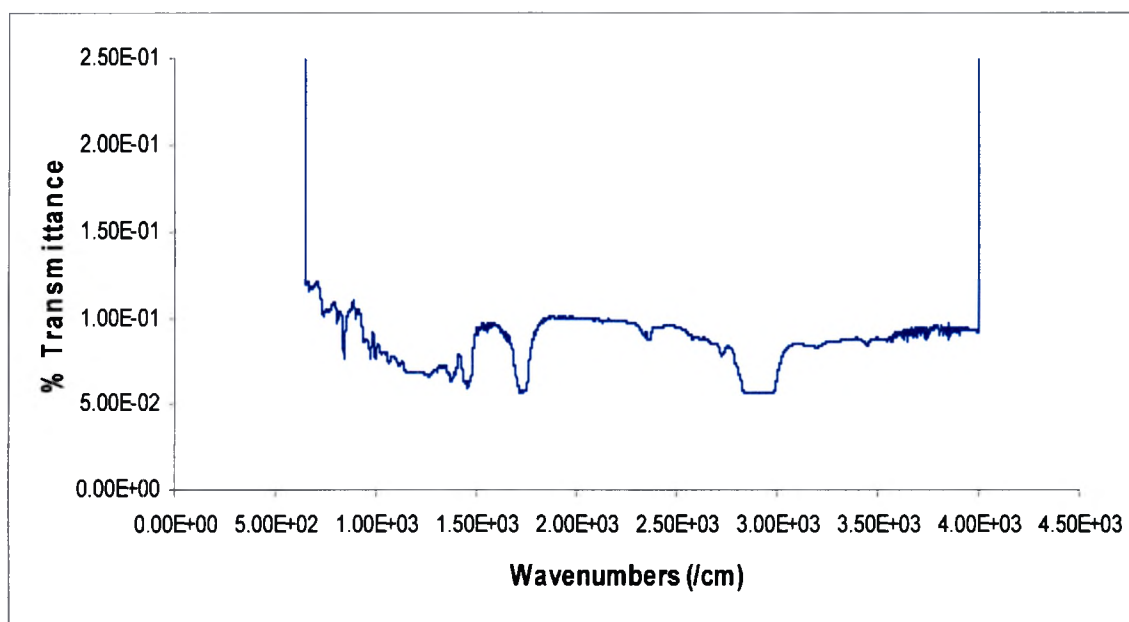


Figure 17. Transmittance Spectrum for SbSI at 16 °C.

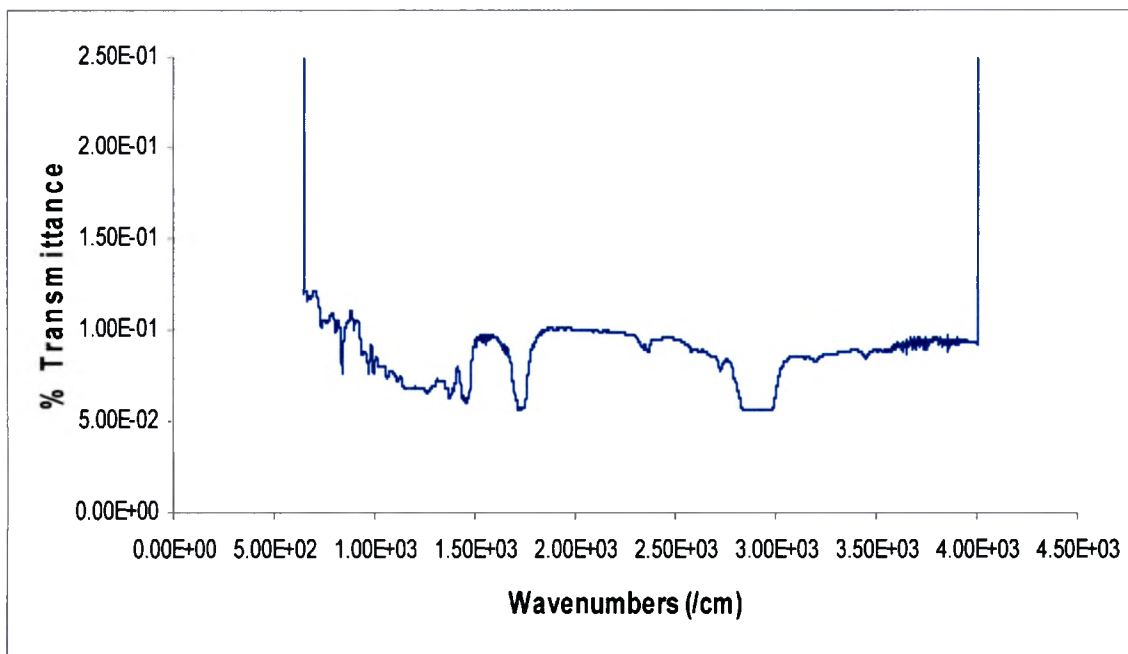


Figure 18. Transmittance Spectrum for SbSI at 17 °C.

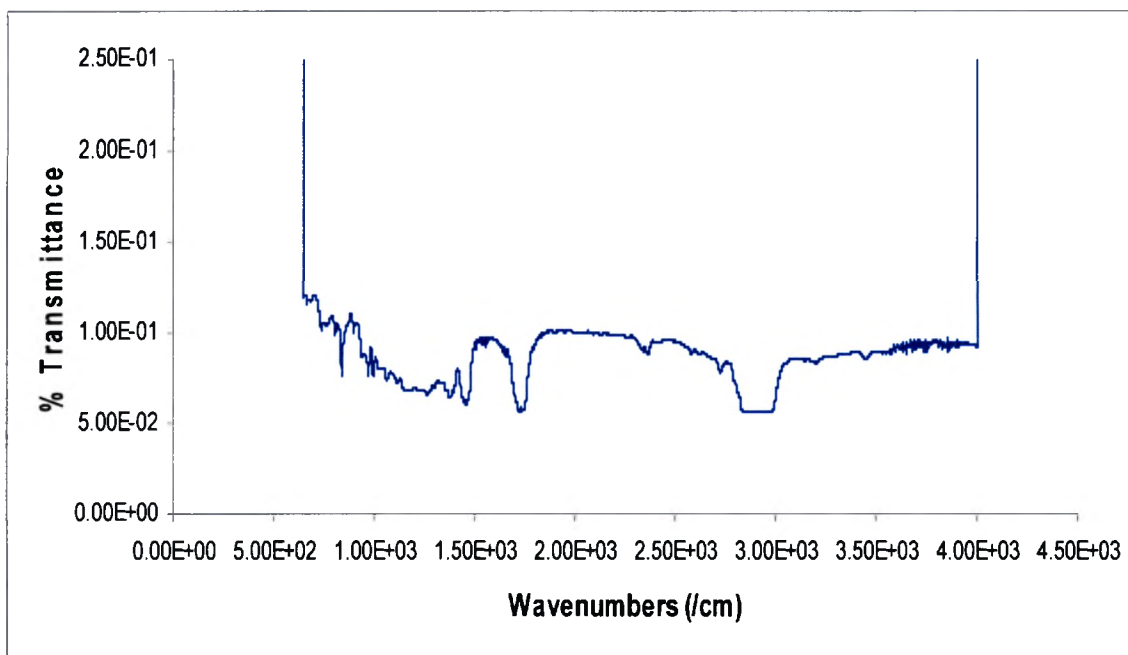


Figure 19. Transmittance Spectrum for SbSI at 18 °C.

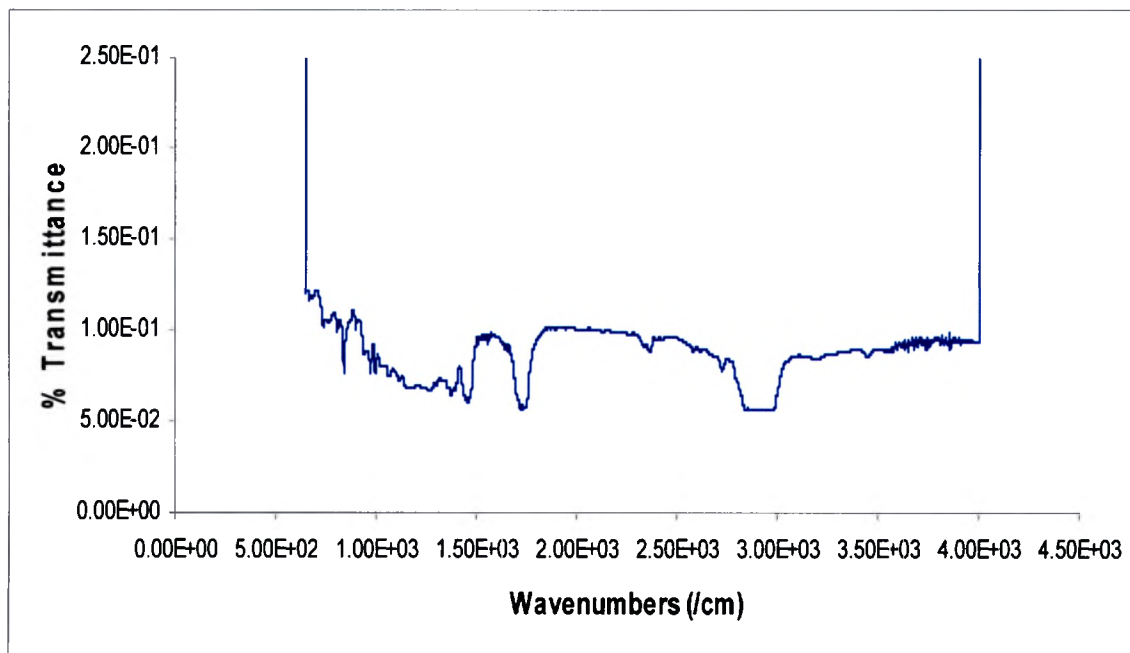


Figure 20. Transmittance Spectrum for SbSI at 19 °C.

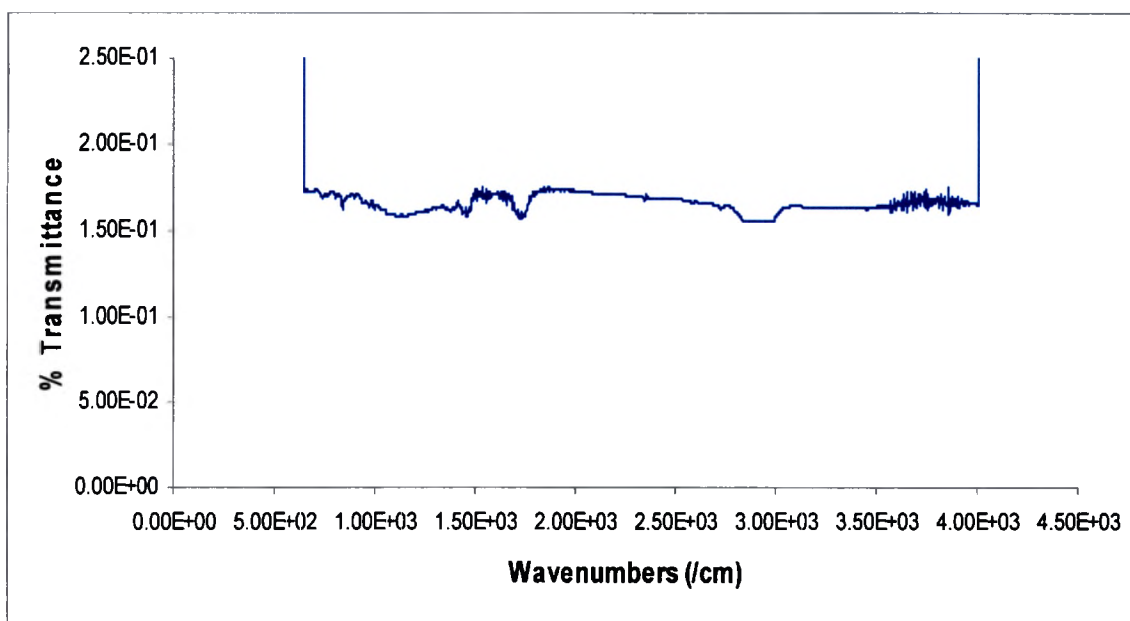
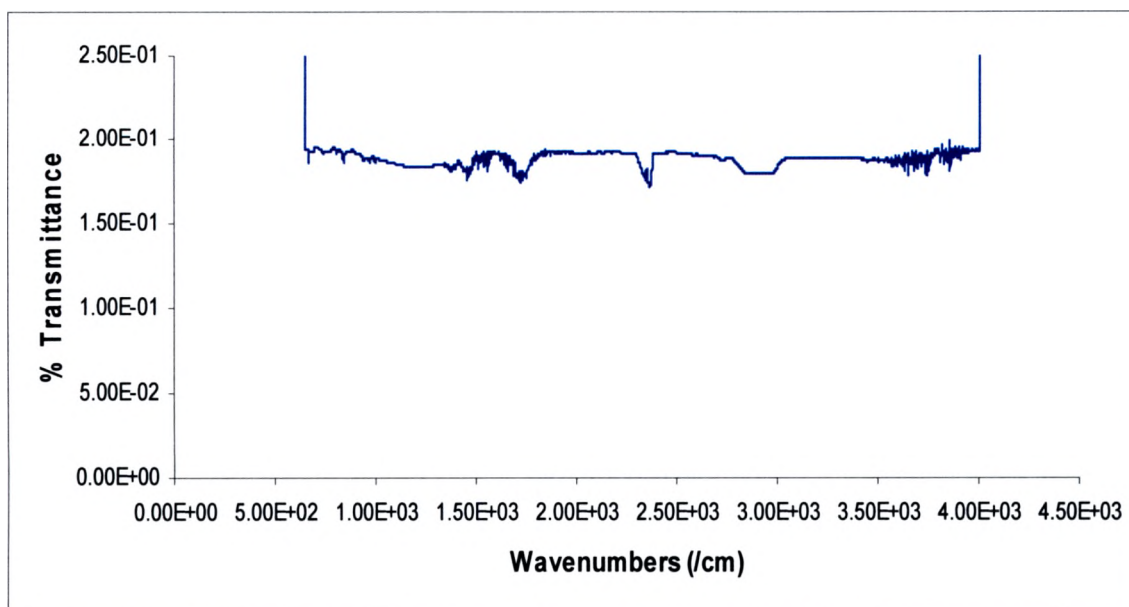
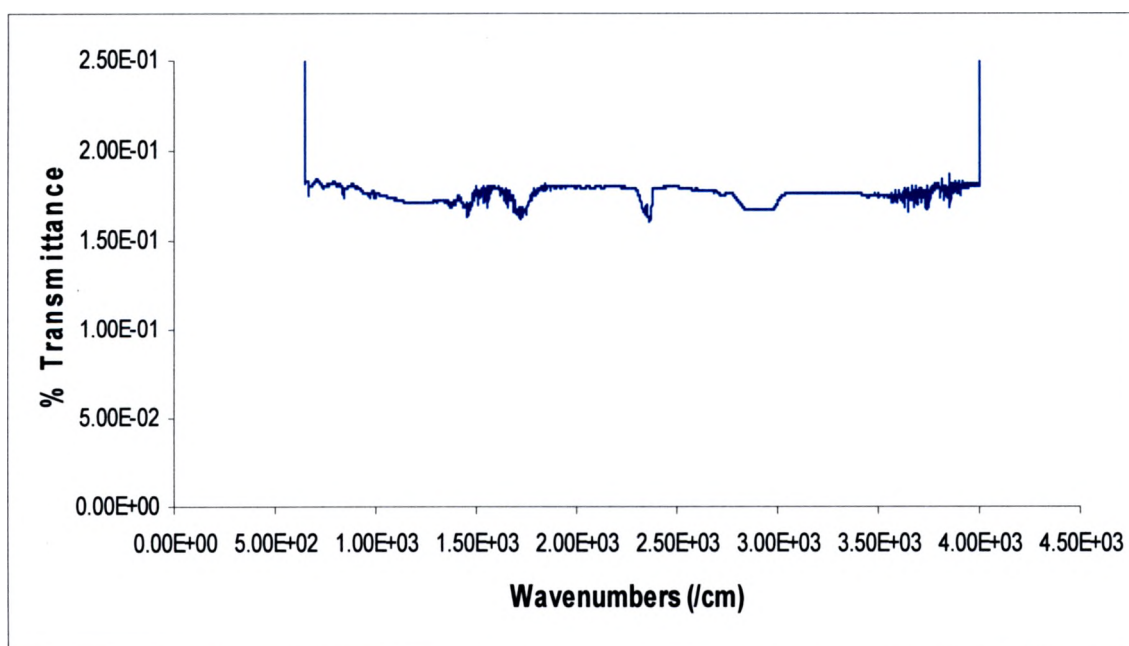


Figure 21. Transmittance Spectrum for SbSI at 20 °C.



**Figure 22. Transmittance Spectrum for SbSI at 21°C.**



**Figure 23. Transmittance Spectrum for SbSI at 22 °C.**

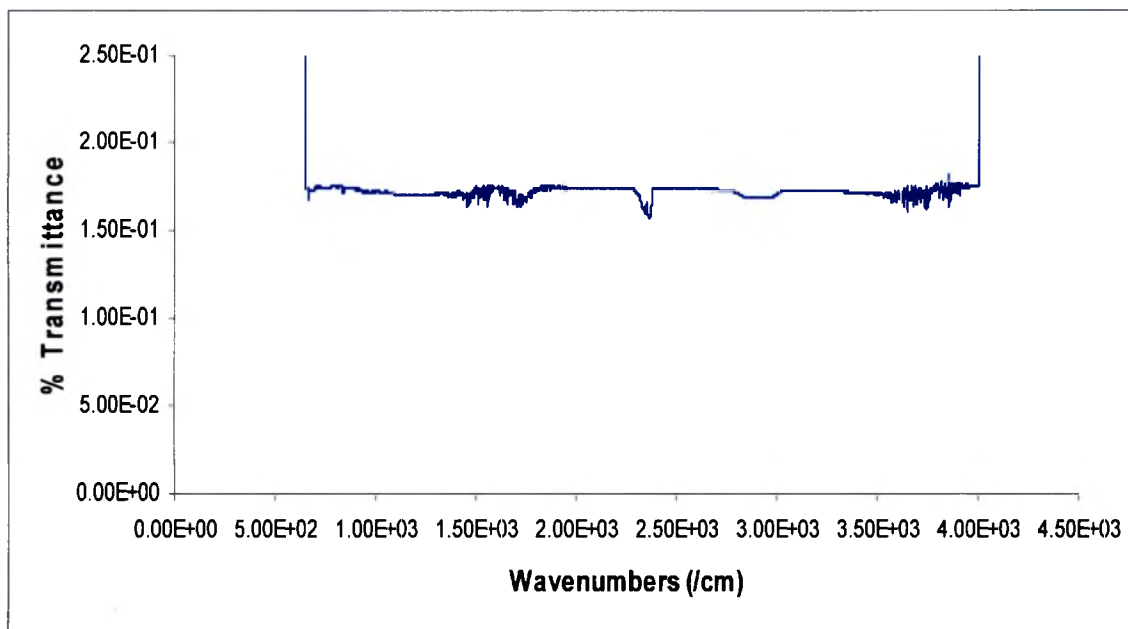


Figure 24. Transmittance Spectrum for SbSI at 23 °C.

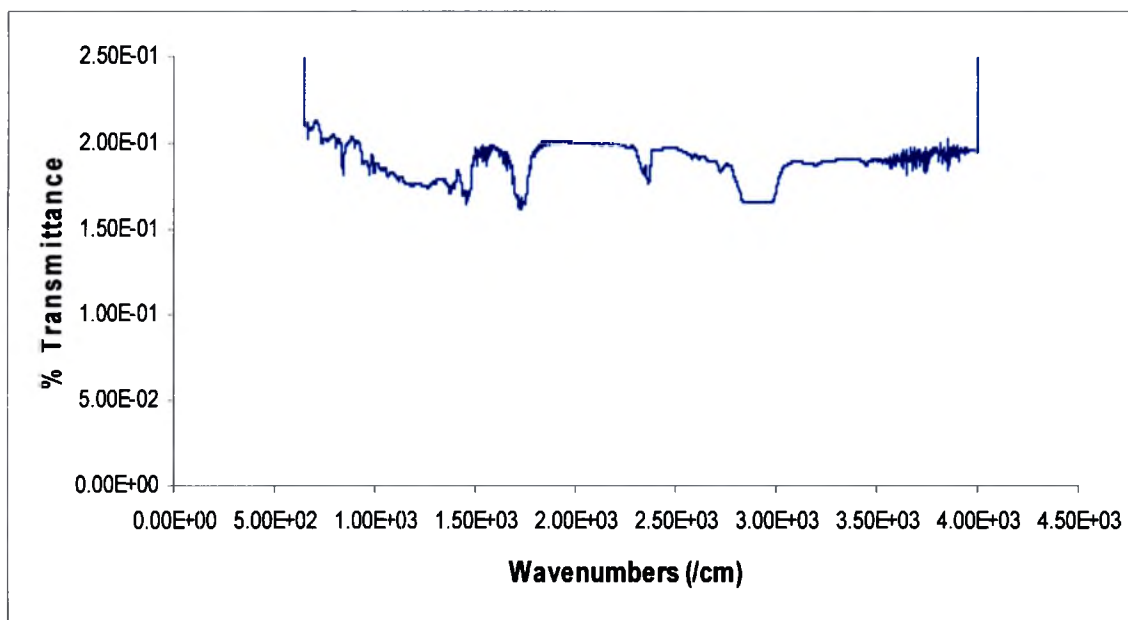


Figure 25. Transmittance Spectrum for SbSI at 24 °C.

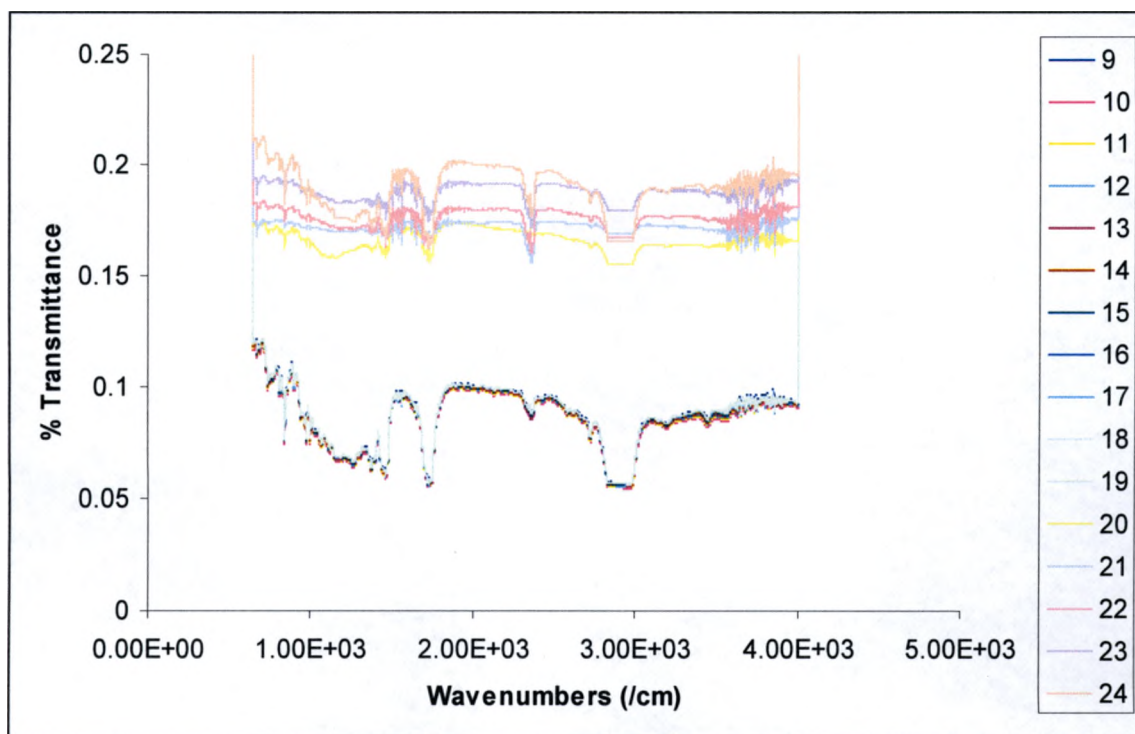


Figure 26. Transmittance Spectrum for SbSI from 9 °C to 24 °C.

## CHAPTER 5

### RESULTS AND CONCLUSION

Analysis of the data allows us to draw some conclusion about the general characteristics of a SbSI film. First; the transmittance is seen to be dependent on temperature, which predicts that SbSI film can be used as an infrared detector. This is because as the temperature increased towards the Curie temperature, the transmittance also increased. In effect, the response of SbSI film to infrared radiation increases with temperature, and it is more pronounced after the Curie temperature. Second; since refractive index is a physical property that is dependent on temperature and wavelength of the light we can say that a pyro-optic property is observed, that is a pyro-optic coefficient was able to be estimated due to the variation of transmittance with temperature. Third; the ferroelectric property of a crystallographic phase change, which causes a different transmittance rate is observed. This is because, for a ferroelectric material, at above the Curie temperature, there is a crystallographic phase change. Fourth; the SbSI film transmittance spectrum seems to reach a non-zero minimum. This minimum is dependent upon temperature.

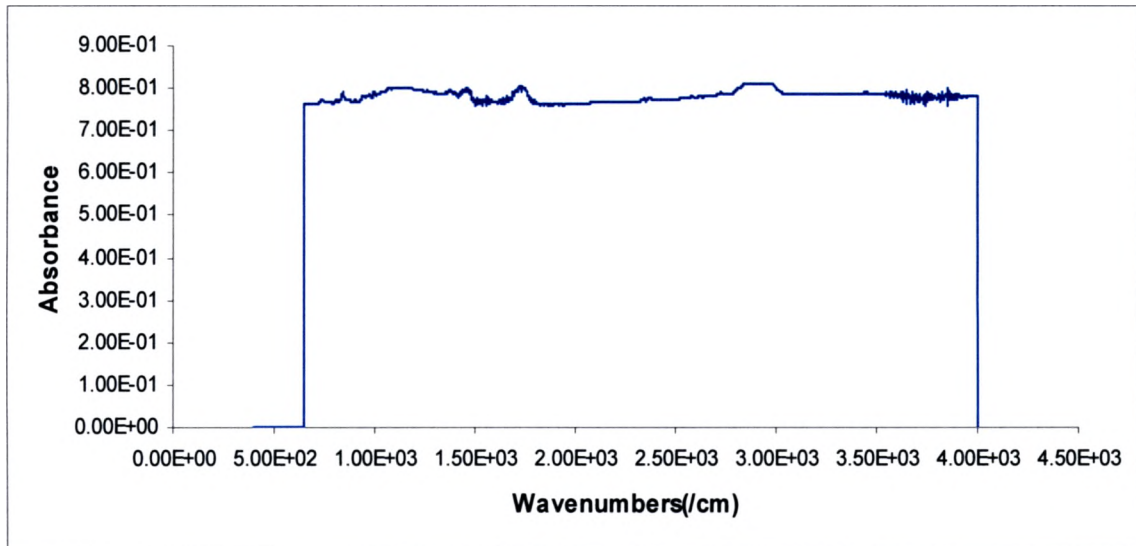
From the transmittance spectrum (Fig. 25) which compares all the spectra from 9 °C to 24 °C, the % transmittance observed increases by very small increments for 9 °C through to 19 °C, which appears to be almost overlapping. This increment becomes more visible after the 19 °C temperature. This is due to the fact that for ferroelectric materials, above the Curie temperature ( $T_C$ ) there is a crystallographic phase change from an asymmetrical, non-centrosymmetric structure to a centrosymmetric crystal structure, thus losing its spontaneous polarization. This change was expected to be observed at around 19 °C which happens to be the Curie temperature for SbSI film, but it occurred at 20 °C. Below the Curie temperature, the variation of transmittance with temperature was observed to be in the range of approximately  $8.83 \times 10^{-6} - 7.08 \times 10^{-4} \text{ } ^\circ\text{C}^{-1}$ , which predicts a smaller pyro-optic coefficient. After the Curie temperature, the transmittance variation was observed to be in the range of  $6.92 \times 10^{-2} - 1.20 \times 10^{-1} \text{ } ^\circ\text{C}^{-1}$ , which predicts a much higher pyro-optic coefficient compared to when it was below the Curie temperature. With these transmittance variations with temperature, the pyro-optic coefficient can be estimated to be around  $7.08 \times 10^{-4} \text{ } ^\circ\text{C}^{-1}$  below the Curie temperature and  $0.12 \text{ } ^\circ\text{C}^{-1}$  above the Curie temperature. This gives SbSI film and pyro-optic detectors in general an advantage over photon detectors and pyroelectric detectors. This is because photon detectors must be cooled to liquid nitrogen temperature (77K) for efficient operation, while pyroelectric detectors also have shortcomings such as electronic noise due to metallic contacts to pixel in the array. One general feature in the data which must be pointed out is that at around  $3500 \text{ cm}^{-1}$  to  $4000 \text{ cm}^{-1}$ , the spectra becomes a little noisy. This is due to an increasingly poor signal to noise ratio with increasing wavenumbers.

## **Suggestions**

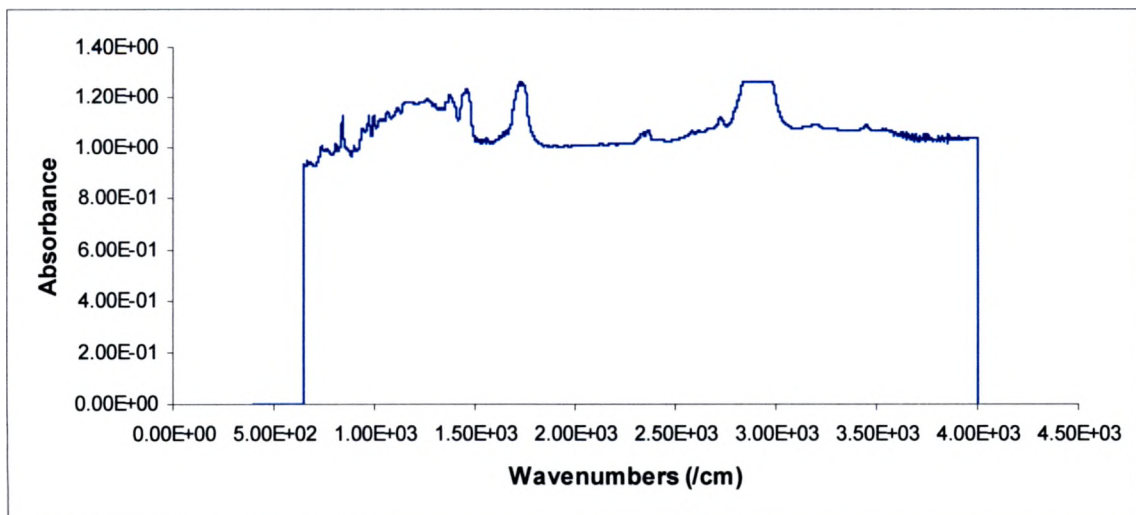
The author suggests that further work should include working with different thicknesses of SbSI film, so that it can be established as to how varying thickness of the film contributes to the transmittance of infrared and also the pyro-optic properties. The dipping of the cryogenic coldfinger in ice to lower the temperature before attaching the sample to it did not really help matters with regards to accurately measuring the spectrum at varying temperatures, so a different way of varying the temperature will help a lot in attaining very accurate results.

## APPENDIX

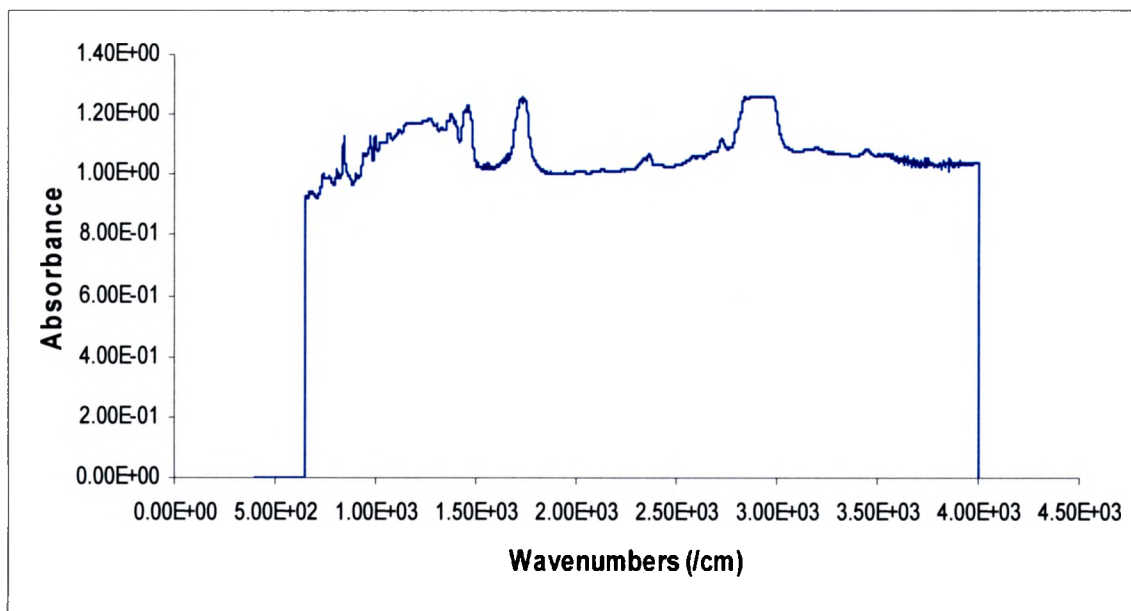
### Absorbance Spectra for SbSI at various temperatures



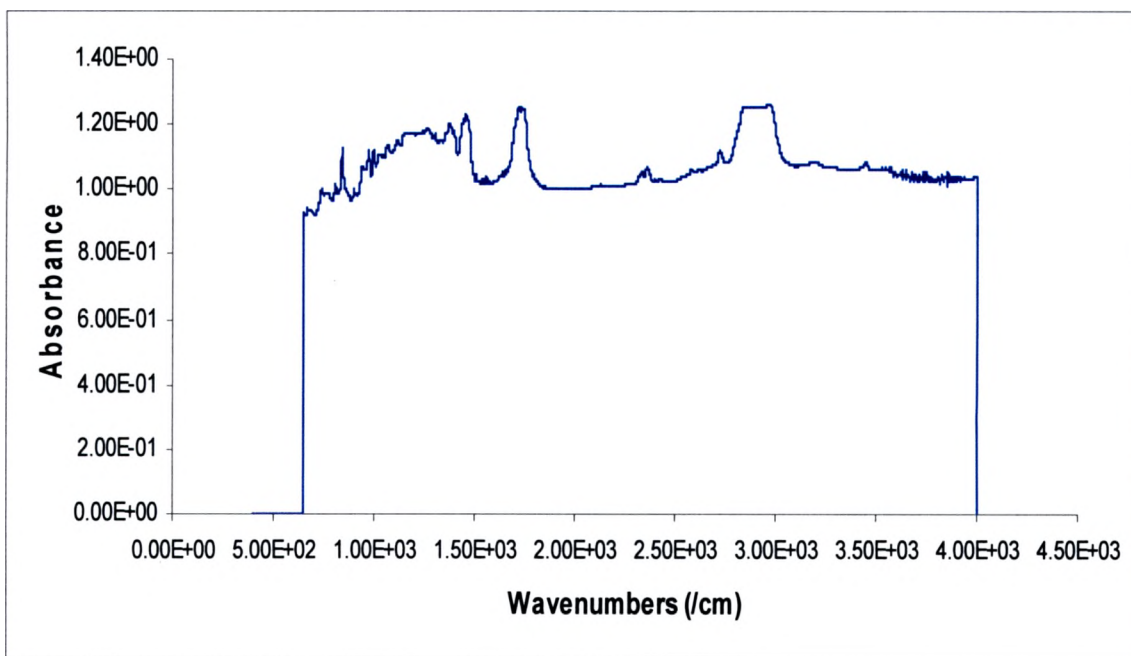
Absorbance Spectrum at 9°C



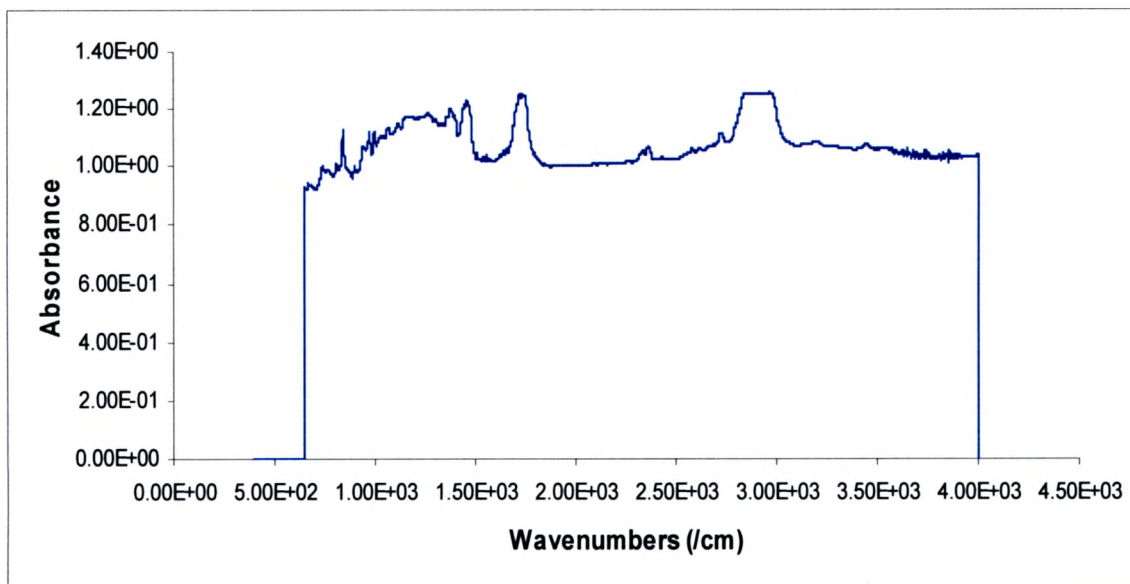
Absorbance Spectrum at 10 °C



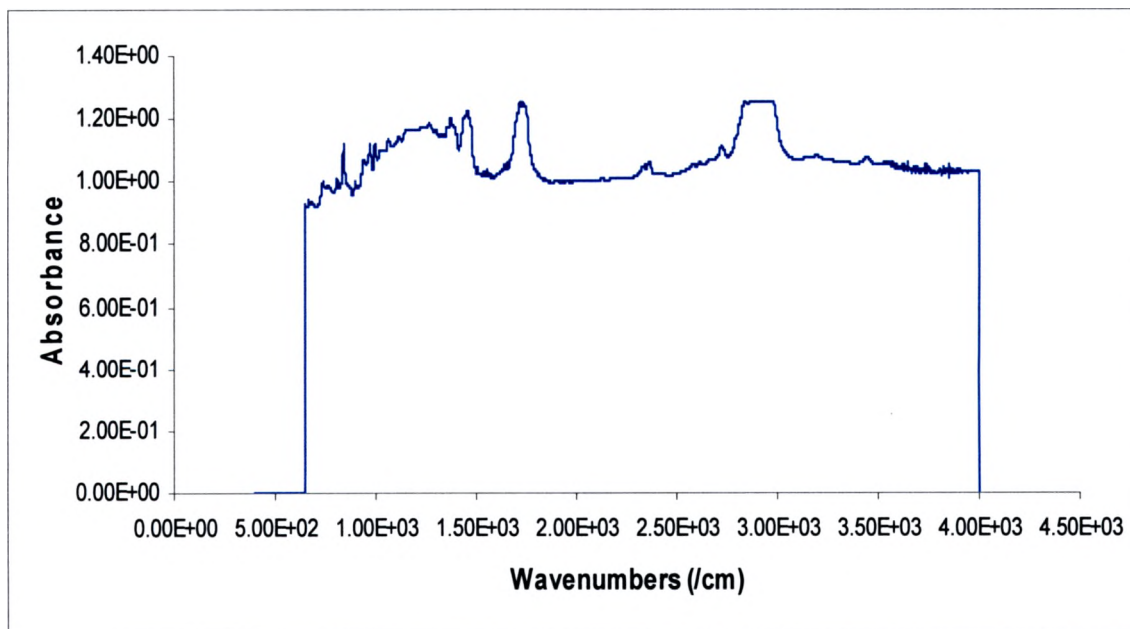
Absorbance Spectrum at 11 °C



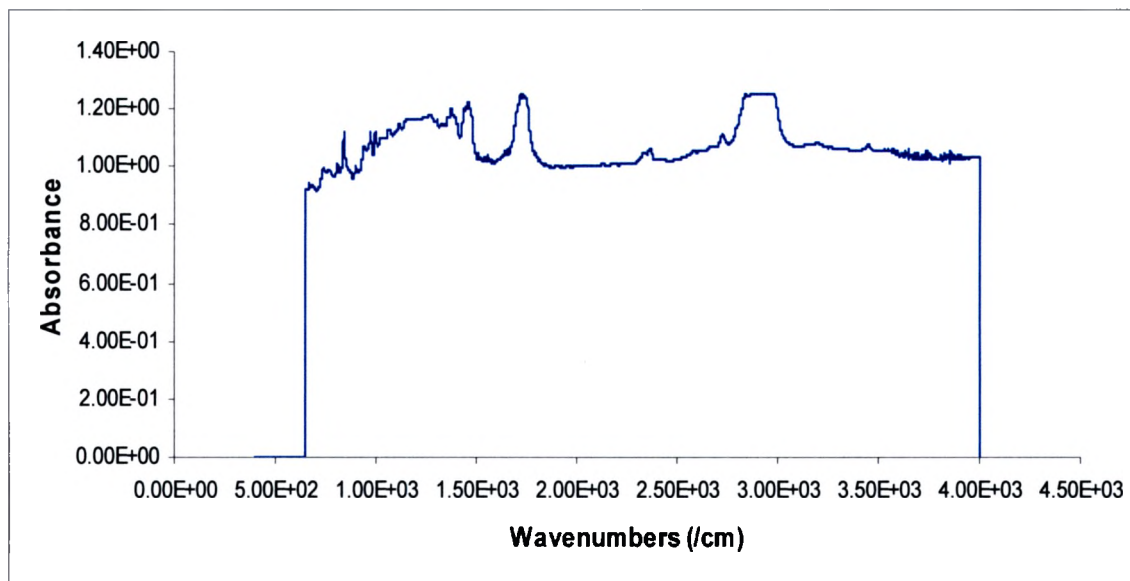
Absorbance Spectrum at 12 °C



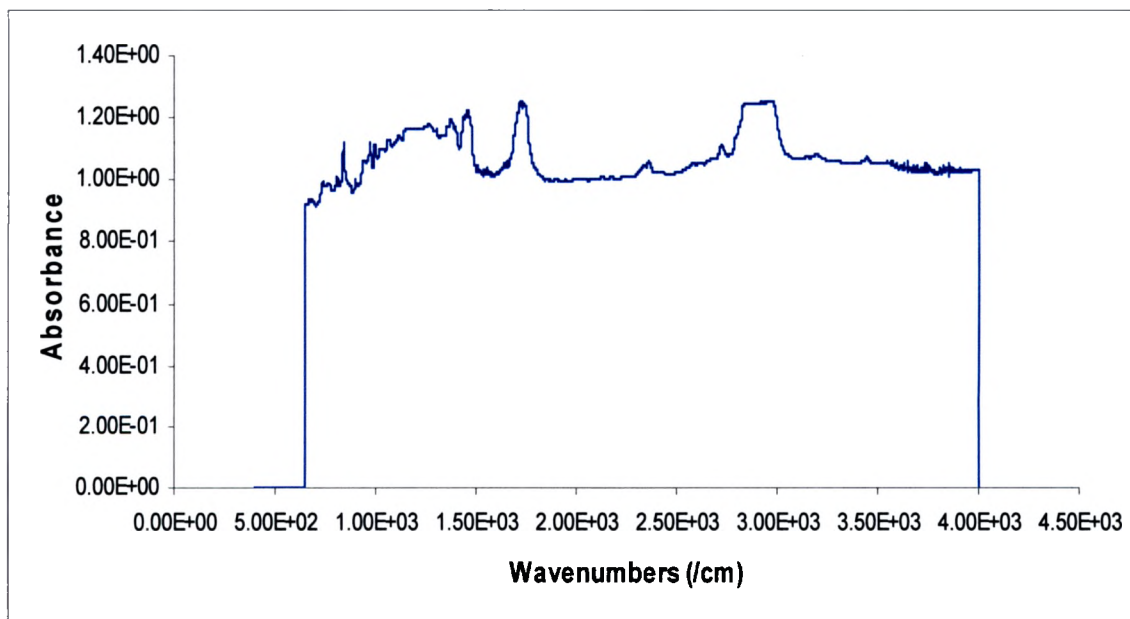
Absorbance Spectrum at 13 °C



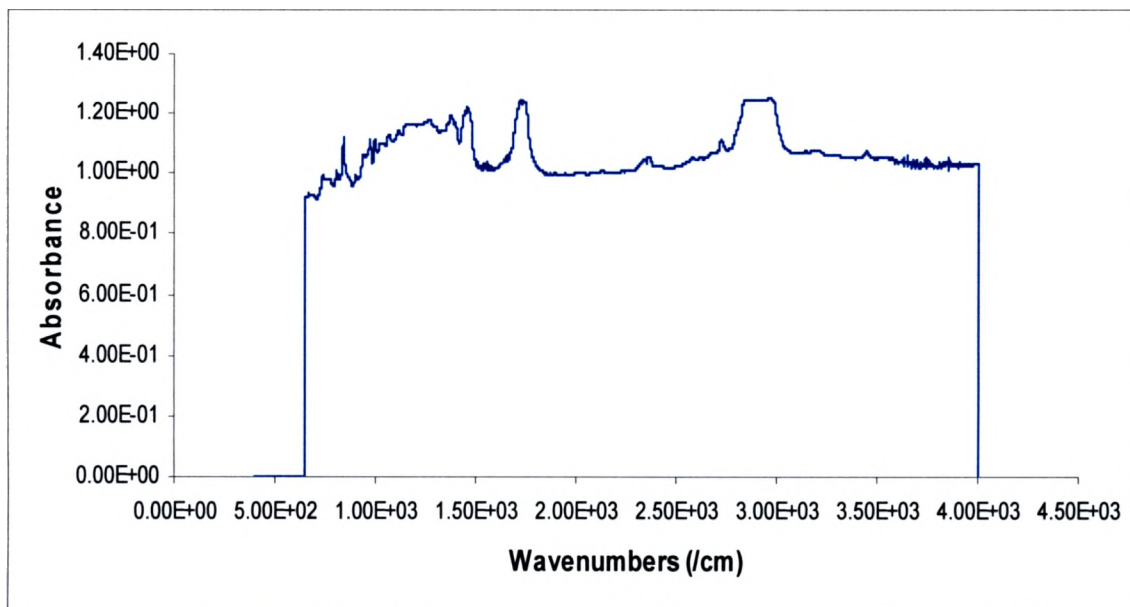
Absorbance Spectrum at 14 °C



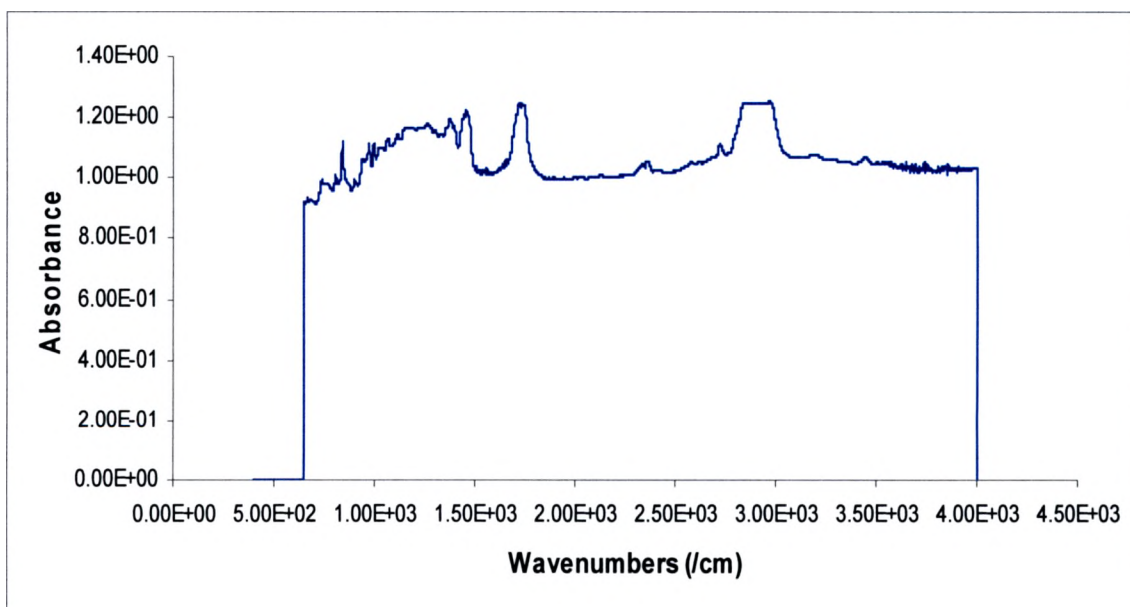
Absorbance Spectrum at 15 °C



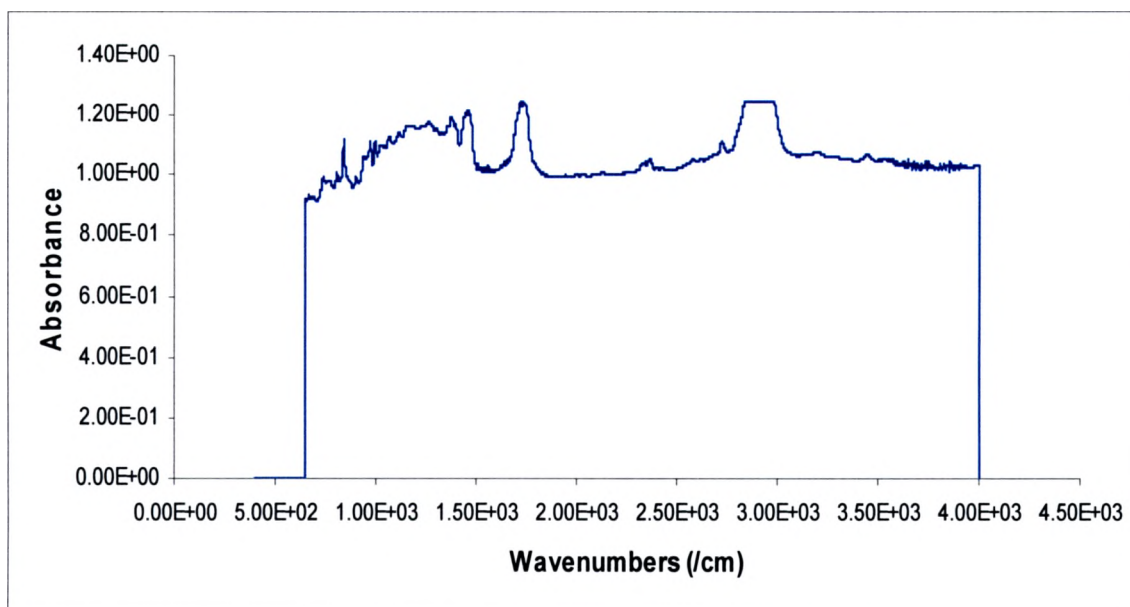
Absorbance Spectrum at 16 °C



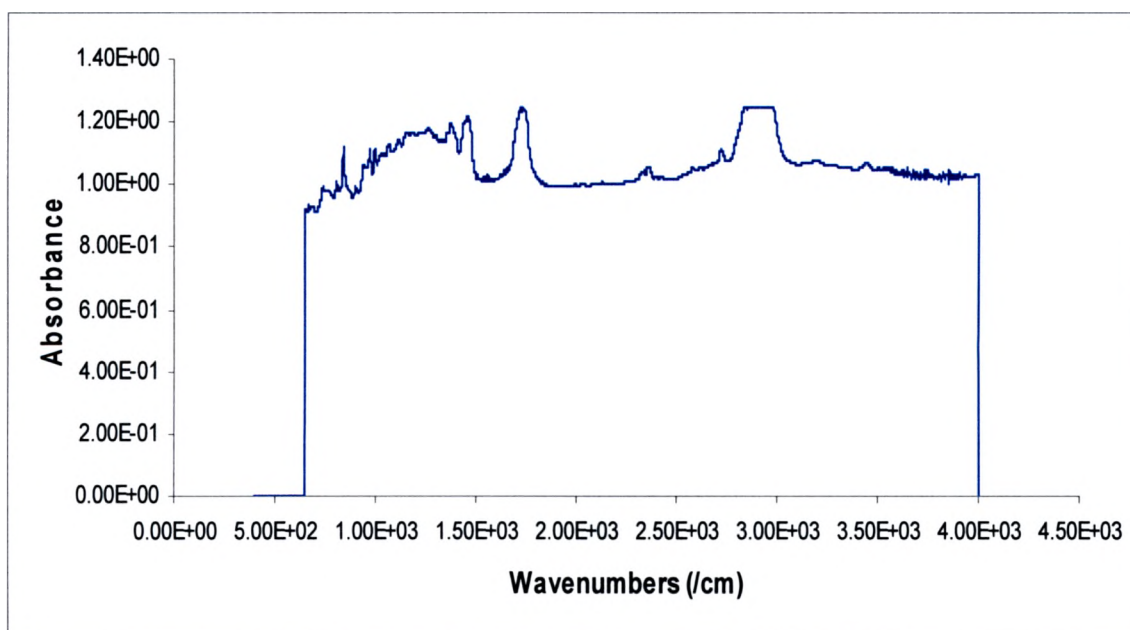
**Absorbance Spectrum at 17 °C**



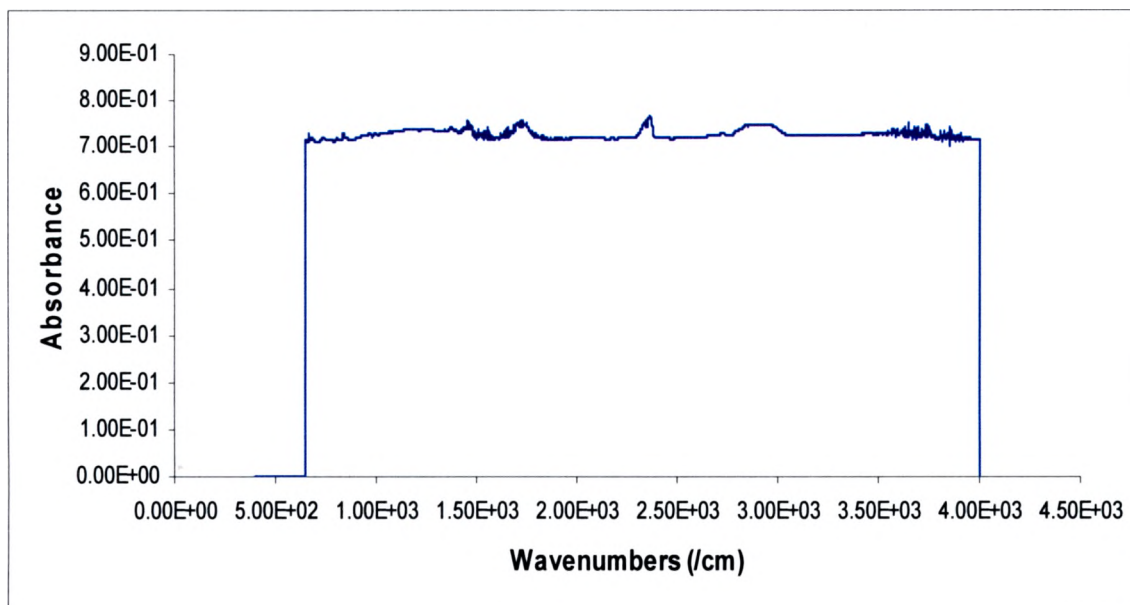
**Absorbance Spectrum at 18 °C**



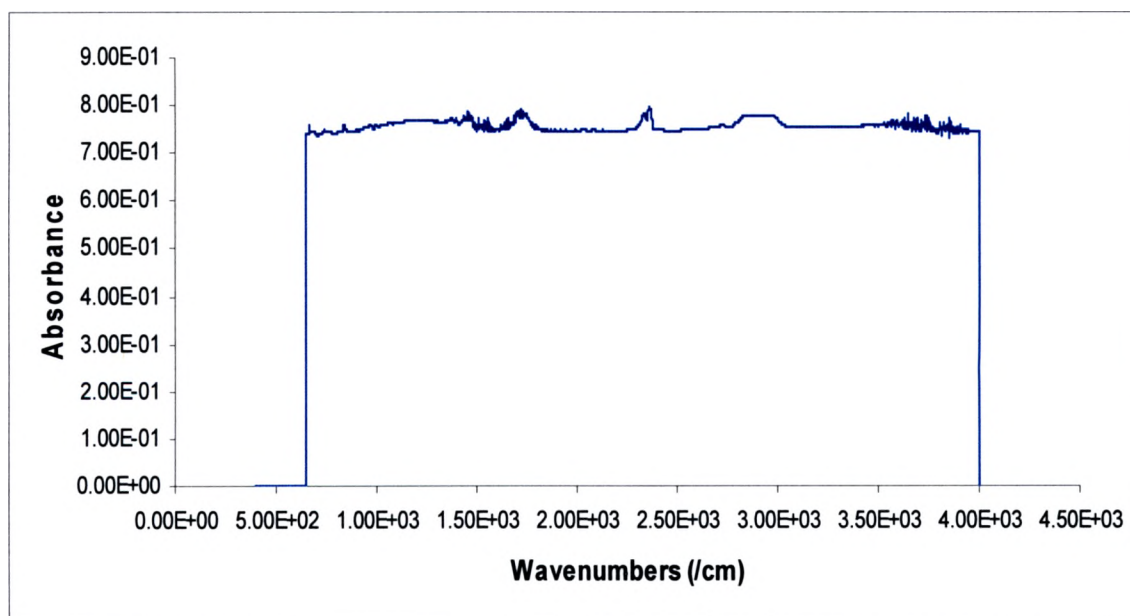
Absorbance Spectrum at 19 °C



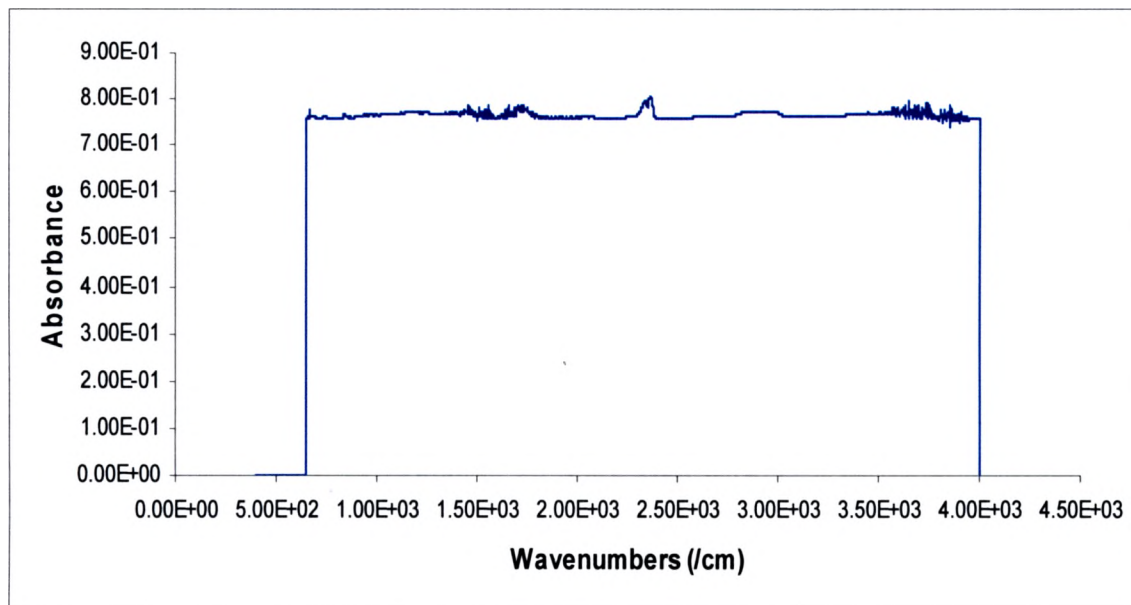
Absorbance Spectrum at 20 °C



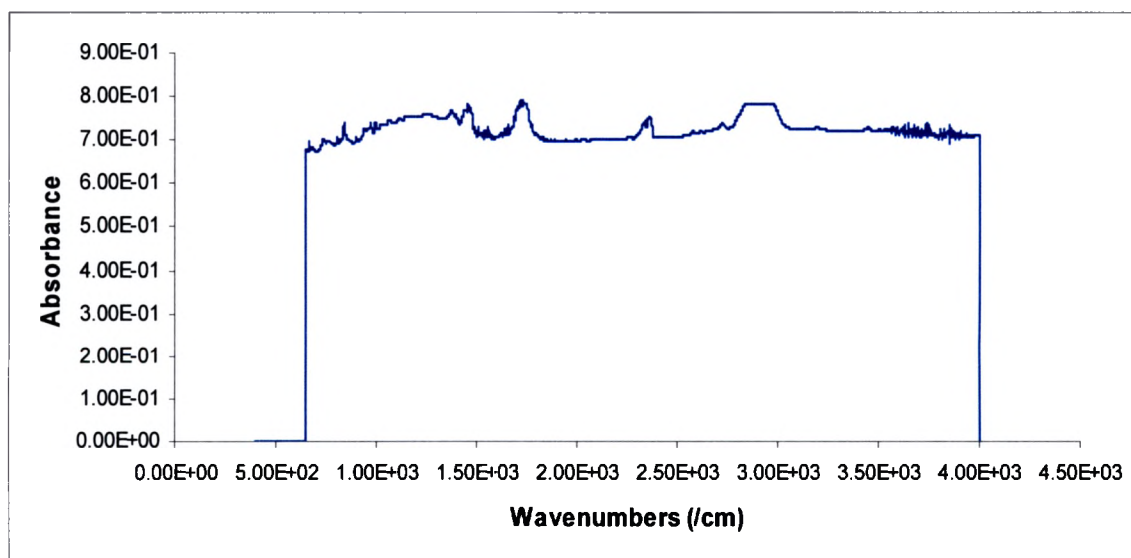
Absorbance Spectrum at 21 °C



Absorbance Spectrum at 22 °C



**Absorbance Spectrum at 23 °C**



**Absorbance Spectrum at 24 °C**

## REFERENCES

1. E. Gerzanich, V. Fridkin; Ferroelectric of  $A^V B^VI C^VII$  Type; Izd. Nauka, Moscow (1982).
2. R. K. Pandey; University of Alabama, Tuscaloosa; Manuscript # 118 for John Wiley's Encyclopedia of RF and Microwave Engineering.
3. Charles Kittel; Introduction to Solid State Physics (7<sup>th</sup> Edition); John Wiley and Sons Inc., New York; pp 443.
4. S. O. Kassap; Principles of Electronic Materials and Devices (2<sup>nd</sup> Edition); (McGraw Hill, 2002); pp 567-568.
5. Dieter K. Schroder; Semiconductor Material and Device Characterization; (John Wiley & Sons, Inc.); pp 601.
6. Sumner P. Davis, Mark C. Abrams, James W. Brault; Fourier Transform Spectrometry; (Academic Press, 2001); pp 11.
7. Brian C. Smith; Fundamentals of Fourier Transform Infrared Spectroscopy; (CRC Press); pp 26.
8. Brian Smith; Infrared Spectral Interpretation, A systematic approach; (CRC Press LLC., Copyright 1999); pp 3-6.
9. D. Skoog, D. West; Principles of Instrumental Analysis; (Holt, Rienhart and Winston Inc. Copyright 1971); pp 131-168.
10. J. Coates; Interpretation of Infrared Spectra, A practical Approach; (John Wiley & Sons Ltd., Chichester, 2000); pp 2-10.
11. Brian C. Smith; Infrared Spectral Interpretation (A systematic approach); (CRC Press, 1999); pp 14.
12. E. Fatuzzo, G. Harbeke, W. J. Merz, R. Nitsche, H. Roetschiand, W. Ruppel; Phys. Rev. 127, 2036 (1962).
13. Physica B: Condensed Matter; Volume 371, Issue 1, 15 January 2006; pp 68-73.

14. Journal of Applied Physics; Volume 71, Issue 5, March 1, 1992; pp 2106-2112.
15. Nicolet FT-IR User's Guide (Copyright 2004); pp 61.
16. Brian C. Smith; Fourier Transform Infrared Spectroscopy; (CRC Press, 1996); pp 43-44.

## VITA

Eric Osei-Yiadom was born in Kumasi-Ghana, on March 10, 1980, the son of Emmanuel Osei-Kofi and Florence Osei-Manu. He graduated Prempeh College, a high school in Ghana in 1996. He then completed a Bachelor of Science degree in Physics from Kwame Nkrumah University of Science and Technology-Kumasi-Ghana in 2002. He then moved from Ghana to the United States in 2003 to enter the Materials Physics graduate program at Texas State University-San Marcos in the Spring of 2004.

Permanent Address: 327 West Woods Street, Apt 501

San Marcos, TX 78666

This thesis was typed by Eric Osei-Yiadom.